International Journal of Geosciences, **2012, 3, 525-548**
http://dx.doi.org/10.4236/ijg.2012.33055 Published Online July 2012 (http://www.SciRP.org/journal/ijg)

Geochemistry and Geochronology of Peraluminous High-K Granitic Leucosomes of Yaoundé Series (Cameroon): Evidence for a Unique Pan-African Magmatism and Melting Event in North Equatorial Fold Belt

Timoleon Ngnotue[1,2*], Ganno Sylvestre[2], Nzenti Jean Paul[2], Schulz Bernhard[3], Tchaptchet Tchato Depesquidoux I[2], Suh Cheo Emmanuel[4]
[1]Department of Geology, University of Dschang, Dschang, Cameroon
[2]Department of Earth Sciences, University of Yaoundé I, Messa, Yaoundé
[3]Institut für Mineralogie, Technische Universität Bergakademie, Freiberg, Germany
[4]Department of Geology, University of Buea, Buea, Cameroon
Email: [*]tngnotue@yahoo.fr, lpgsdor@yahoo.com

Received January 2, 2012; revised March 6, 2012; accepted May 5, 2012

ABSTRACT

Geochemical and geochronological studies have been carry out on the leucosomes of Yaoundé series with the aims to identify the magma sources and to indicate their production periods and emplacement within the formations of the Pan-African North-Equatorial Fold Belt (PANEFB) in Cameroon. The Yaoundé series belongs to the Southern domain of the PANEFB and it is composed of migmatites in which two types of granitic leucosomes (*in situ* leucosomes and injected leucosomes) have been distinguished. These rocks display characteristic of calc-alkaline (*in situ* leucosomes) and high-K calc-alkaline to shoshonitic series (injected leucosomes). All the rocks are peraluminous with *in situ* leucosomes conform to S-type and injected leucosomes conform to I- and S-type granitoids. Major and trace elements composition reveal that *in situ* leucosomes derived from the partial melting of the host metapelite whereas injected leucosomes derived from the melting of metagreywacke. These sources are similar to those of granitoids from central and northern domains of the PANEFB. Th-U-Pb dating by electron microprobe (EMP) and LA-ICP-MS U-Pb dating on zircon have been used to constraints the melting event and emplacement of leucosomes in Yaoundé series. Th-U-Pb monazite dating, undertaken in two samples of leucosomes, gives two groups of monazite ages. The older group gives an age of 658 Ma whereas the age of younger group is 592 Ma. U-Pb dating of zircons from the leucosomes reveals a Pan-African age ranging from 626 to 654 Ma whereas zircons from metapelitic host rock reveal the overprinting of an early Pan-African event 911 - 1127 Ma on Palaeoproterozoic (2127 Ma) inheritance. These data clearly indicate that the host rocks of leucosomes of Yaoundé series have been firstly metamorphosed during Tonien-Stenien period (911 - 1127 Ma) and reveal the existence of extended unique melting event (592 and 658 Ma) in the Yaoundé series which is contemporaneous with the magmatism responsible for the emplacement of granitoids in the other domains of the PANEFB.

Keywords: Pan-African North-Equatorial Fold Belt; Yaoundé Series; EMP Monazite Dating; LA-ICP-MS U-Pb Dating; Leucosomes; Peraluminous; Melting Event; Magmatism

1. Introduction

Peraluminous magmatism is largely reported in the collisional belt. However, this magmatism is also observed, but in least proportion, in the passive margin setting where it is expressed by volcanic tuffs [1,2]. The study of metamorphic and igneous rocks provides important information on the magmatic processes which took place in the continental lithosphere, especially in the collisional belt. In this type of orogeny, there is a strong relation between metamorphism, deformation, melting and/or magmatism. The study of the granitic melt is of fundamental importance for the understanding of the main processes of genesis and evolution of the continental crust and notably of the palingenesis.

Till date, peraluminous magmatism in Cameroon is only reported in the northern and the central domains of the Pan-African North-Equatorial Fold Belt (PANEFB). The study of the leucosomes in the migmatites of Yaoundé in the southern domain of the PANEFB has revealed their granitic composition and their peralumi-

[*]Corresponding author.

nous affinity. The ubiquity of the magmatism in the PANEFB, which spreads more than 500 km, from the northern domain to the southern domain, can be assigns either to the existence of a unique melting event along the belt, or to distinct melting episodes. Indeed, the uniqueness of metamorphic and tectonic phenomena throughout the PANEFB was demonstrated by many authors [3-5].

This paper presents the results of geochemical and geochronological studies of the leucosomes of the southern domain of the Pan-African North-Equatorial Fold Belt. These results, compared to those obtained on the granitoids of the northern and the central domains, allow us 1) to identify the magma sources all over the Pan-African North-Equatorial Fold Belt and 2) to indicate their production periods (ages) and emplacement within the formations of the PANEFB in Cameroon.

2. Regional Geological Setting

The Yaoundé series belongs to the Southern domain of the Pan-African North-Equatorial fold belt and is situated in the northern edge of the Congo craton (**Figure 1**). It is composed of intensely deformed metasedimentary and meta-igneous rocks [6]. The metasedimentary rocks are made up of chlorite schist, garnet and/or kyanite bearing micaschist and garnet and kyanite bearing gneisses. The protoliths of these rocks are shale and greywacke deposited in an intracontinental rift context or thinned margin [6,7]. These metasediments are locally intruded by diorite and/or granodiorite and metamorphosed under HP-HT conditions (T = 750˚C - 800˚C, P = 0.9 - 1.3 GPa; [6, 8]) at 620 ± 10 Ma (U-Pb age on zircon; [9]) or at 616 Ma (U-Pb age on zircon and Sm-Nd; [10]) and or between 613 ± 33Ma and 586 ± 15Ma (Th-U-Pb age on monazite; [11]).

The rocks of this unit have been affected by two major phases of deformation associated to the metamorphism [6, 12,13]: 1) the D_1 phase is marked by a compositional bedding (So/S_1) parallel to the preferential orientation of the phyllosilicates and ended by the formation of the high

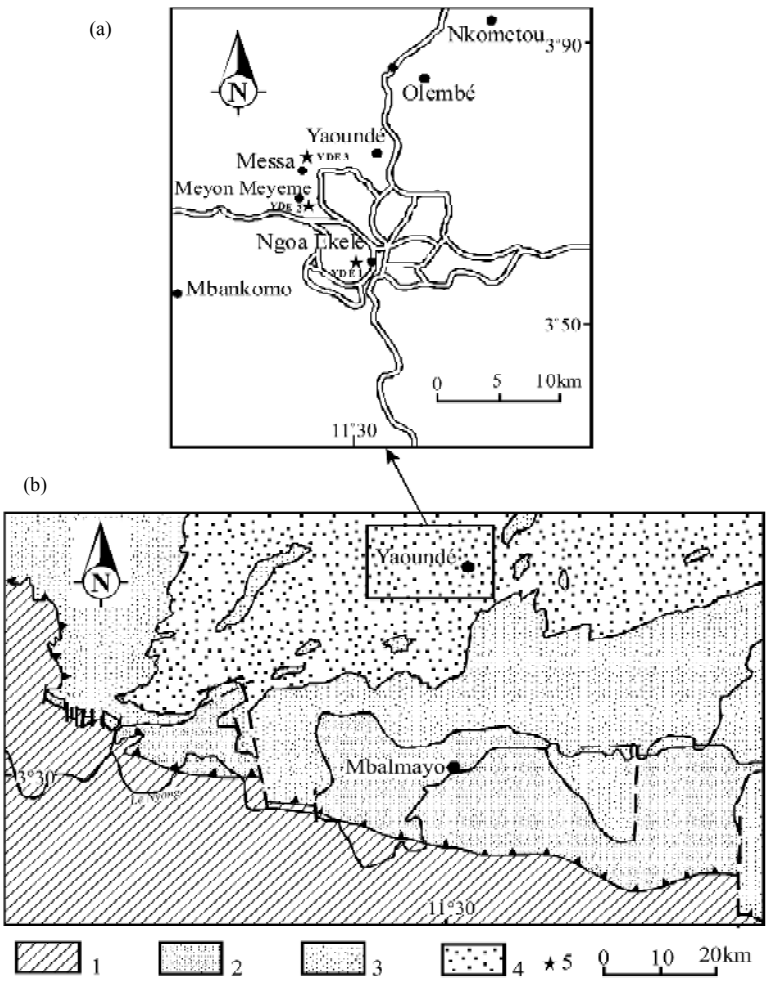

Figure 1. (a) Location map of the study area; (b) Geological map of Yaoundé group (adapted from [6]). 1: Congo Craton; 2: Mbalmayo series; 3 and 4: Yaoundé series (Garnet micaschist and migmatitic gneisses, respectively); 5: Sampling site.

pressure granulite-facies assemblage and the beginning of partial melting; 2) the D_2 event is a compressionnal phase marked by the intrusion of mafic rocks, the *in situ* partial melting, the injection of the quartzo-feldspathic melt along the C_2 shear plane and by a southward thrusting of the rocks of this series onto the Archean Congo Craton. The migmatisation develops mainly during this second phase.

In addition to the southern domain, the Pan-African North-Equatorial Fold Belt is made of two other geodynamic domains (the northern and the central domains, **Figure 2**):

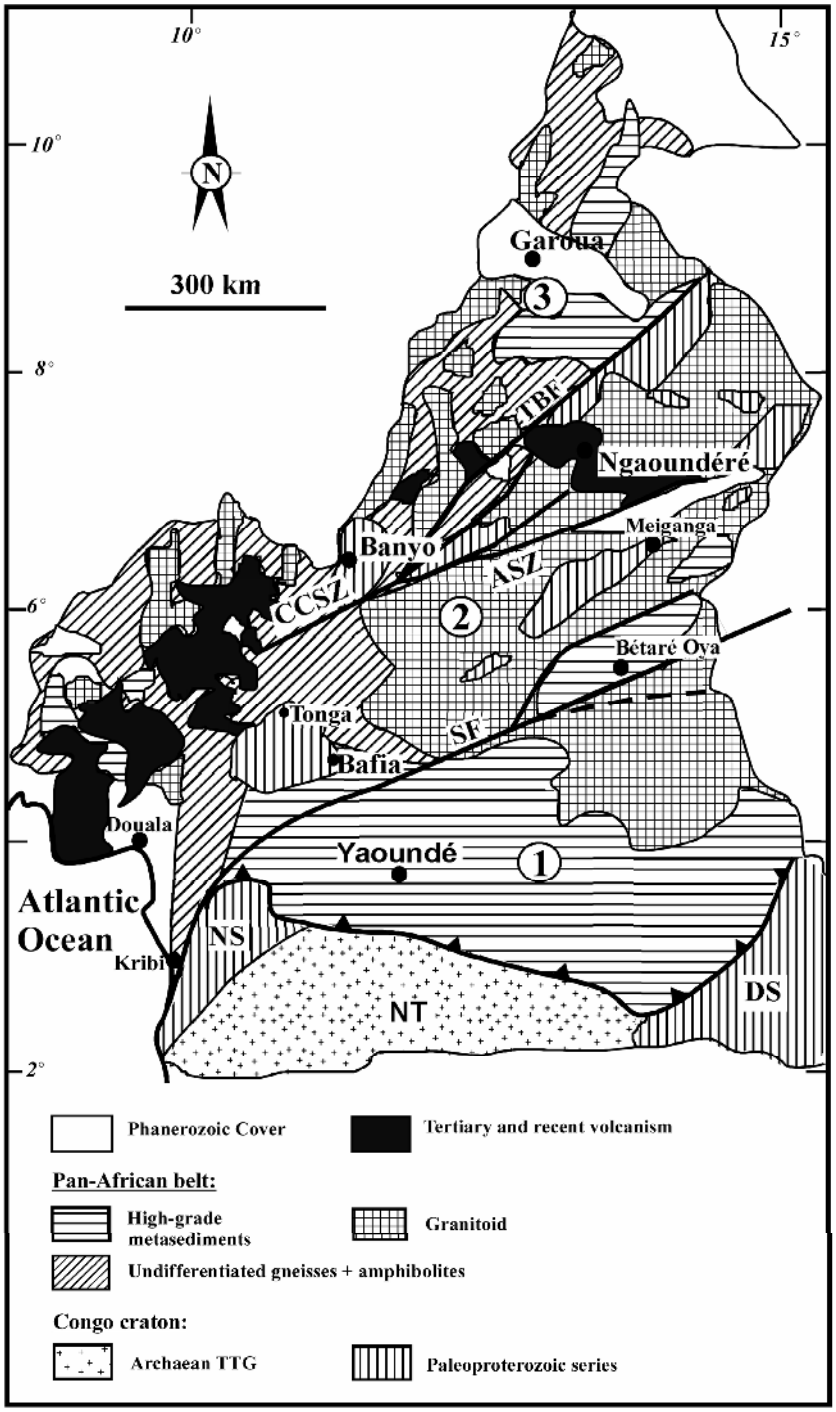

Figure 2. Geological map of Cameroon (adapted from [4]) showing the localization of the Yaoundé area and the three main lithotectonic domains of PANEFB: 1) Southern domain; 2) Central domain; 3) Northern domain. CCSZ: Central Cameroon Shear Zone); SF: Sanaga Fault; TBF: Tibati Banyo Fault; NT: Ntem Complex; DS: Dja Series; NS: Nyong Series.

1) The northern domain, with polyphase and polycyclic evolution [14-18], consists of metavolcanite of tholeiitic and alkaline affinities associated with metasediments (Poli series) and widespread 630 - 660 Ma calc-alkaline orthogneisses interpreted as major episode of accretion [17]. These orthogneisses contain granulitic relics of Palaeoproterozoic age (2100 Ma, [9]).

2) The central domain consists of an assembly of fragments of Paleoproterozoic continental crust recristallised under high-grade granulite facies (850˚C - 900˚C, 10 - 12 Kb) at ca. 2100 Ma [3,19,20] intruded by widespread Pan-African syntectonic granitoids. These granitoids have high-K calc-alkaline to shoshonitic affinities. They are either S-type peraluminous granite [4], or I-type metaluminous to weakly peraluminous granite [21-24] and are derived from the partial melting of the metapelite or metagreywacke sources. Their emplacement age ranges from 558 Ma to 621 Ma [19,21,24-26].

3. Analytical Procedures

3.1. Whole Rock Geochemistry

Samples were collected from fresh outcrops in quarries around Yaoundé. Leucosomes were separated from each other in a set of centimeter-thick slabs cut perpendicular to the foliation of the samples. Major elements, as well as Rb, Sr, Zr, Nb, and Y, were determined by X-ray fluorescence (XRF) spectrometry at the University of Nancy I using the procedure outlined by Govindaraju & Montanari [27]; Th, U and rare earth elements (REE) were determined by inductively coupled plasma emission spectrometry (ICP-ES) and by absorption spectrometry at CRPG, Nancy [28]. Analytical uncertainties are estimated at 2% for major elements, and at 5% or 10% for trace element concentrations higher or lower than 20 ppm respectively. Precision for REE is 5% when chondrite-normalized concentrations are >10 and 10% when there are lower. Samples are normalized to chondrite using the factors presented by Jahn *et al.* [29].

3.2. EMP Method

Analysis of Th, U and Pb for calculation of monazite model ages, as well as for Ca, Si, LREE and Y for corrections and evaluation of the mineral chemistry were carried out on a JEOL JXA 8200 (Chair of Mineralogy, University of Erlangen-Nürnberg) at 20 kV, 100 nA, and a beam size of 5 μm [30]. M1 lines of Th and Pb and the M1 lines for U of a PETH crystal were selected for analysis. Resulting errors (1σ) are typically 1.0%, 0.20% and 1.30% for Pb, Th and U, respectively, based on counting statistics. The lines Lα1 for La, Y, Ce; Lβ1 for Pr, Sm, Nd, Gd and Kα1 for P, Si and Ca were chosen. Orthophosphates of the Smithsonian Institution were used as standards for REE analysis [31,32]. Calibration of PbO was carried out on a vanadinite standard, while U was calibrated on an appropriate glass standard with 5 wt% UO_2. The Madmon monazite [30], dated by SHRIMP at 489 ± 9 Ma and numerous Pb-Pb-TIMS monazite evaporation data at 497 ± 2 Ma, contains ThO_2 at around 10 wt%. The ThO_2 in Madmon was previously determined by LA-ICPMS and by the microprobe at University of Salzburg [33] and was used for calibration of ThO_2 as well as for the control of data. Interference of YLγ on the PbM line was corrected by linear extrapolation after measuring several Pb-free yttrium glass standards as proposed by Montel *et al.* [34]. An interference of ThMγ on UM was also corrected by using a Th-glass standard. Interference of a Gd-line on UMβ needs correction when Gd_2O_3 in monazite is >5 wt%. These parameters matched the analytical problems discussed in [35] in the best way [30]. For each single analysis, a chemical age (CHIME) and a 2σ error based on the Pb counting statistics was calculated. Other possible sources of error, as standardization, matrix effect correction, YLγ-on-PbMα correction and instrumental drift were not taken into account. Therefore the given error on the calculated ages should be considered as a minimum error.

3.3. U-Pb LA-ICP-MS Method

U-Pb isotopic analyses were performed in the geochronology laboratory of the University of Brasilia and followed the analytical procedure described by Buhn *et al*. [36]. Zircon concentrates were extracted from ca. 10 kg rock samples using conventional gravimetric and magnetic techniques at the geochronology laboratory of the University of Brasilia. Mineral fractions were hand picked under a binocular microscope to obtain fractions of similar size shape and colour.

For *in situ* ICP-MS analyses, hand picked zircon grains were mounted in epoxy blocks and polished to obtain a smooth surface. Backscattered electron and cathodoluminescence images were obtained using a scanning electron microscope in order to investigate the internal structures of zircon crystals prior to analysis.

Before LA-ICP-MS analyses, mounts were cleaned with dilute (ca. 2%) HNO_3. The samples were mounted in a specially adapted laser cell and loaded into a new Wave UP213 Nd: YAG laser (λ = 213), linked to a Thermo Finnigan Neptune Multi-collector ICPMS. Helium was used as the carrier gas and mixed with argon before entering the ICP. The laser was run at a frequency of 10 Hz and energy of 34%. In order to avoid down-hole fractionation during ablation, we adopted for a raster scan of about 70 μm in total diameter with a spot size of 30 μm.

Two international zircon standards were analysed throughout the U-Pb analyses. The zircon standard GJ-1

[37] was used as the primary standard in a standard-sample bracketing method, accounting for mass bias and drift correction.

The resulting correction factor for each sample analysis considers the relative position of each analysis within the sequence of 4 samples bracketed by two standard and two blank analyses each [38]. The Temora 2 standard [39] was run at the start and the end of each analytical session, yielding an accuracy around 2% and a precision in the range of 1%. The errors of sample analyses were propagated by quadratic addition of the external uncertainty observed for the standards to the reproducibility and within run precision off each unknown analysis. The instrumental set-up and further details of the analytical method applied are given by Buhn *et al.* [36].

The masses 204, 206 and 207 are measured with ion counters, and ^{238}U was analyzed on a Faraday cup. The signal of ^{202}Hg was monitored on an ion counter for correction of the isobaric interference between ^{204}Hg and ^{204}Pb. The signals during ablation were taken in 40 cycles of 1 sec each. For data evaluation, only coherent intervals of signal response were considered. Data reduction was performed with an Excel spreadsheet developed by one of the authors that considers blank values, zircon standards composition and errors propagation. The ^{204}Pb signal intensity was calculated and corrected using a natural $^{202}Hg/^{204}Hg$ ratio of 4.346. A common Pb correction was applied for zircons with $^{206}Pb/^{204}Pb$ lower than 1000, applying a common lead composition following the Stacey and Kramers model [40]. Plotting of U-Pb data was performed by ISOPLOT v.3 [41] and errors for isotopic ratios are presented at the 2σ level. Because of the statistical treatment applied in calculating Concordia ages, those are more precise than any individual U/Pb or Pb/Pb ages [42] and, in data herein presented, always correspond to less than the 2% accuracy obtained from the intercalibration of the standards. Consequently, the Isoplot calculated errors were modified in order to incorporate this uncertainty level and, hence, represent a more realistic age in terms of the analytical limitations of the method.

4. Results

4.1. Petrography and Mineral Chemistry

Two main types of leucosomes have been distinguished on the basis of petrographic and structural criteria:

1) Injected leucosomes

Injected leucosomes occur in two manners: i) along the C_2 shear zone; ii) as cross-cutting dykes (**Figure 3(a)**). They are observed in both metapelitic gneisses and metabasites where they are sometimes associated with ultramafic dykes. Injected leucosomes are either:

i) fine-grained, composed of ribbons quartz (25% - 30%), large perthitic K-feldspar (Or_{95} Ab_5-Or_{89} Ab_{11}) crystals, euhedral plagioclase (5% - 10%) crystals rarely zoned showing deformed twins (**Figure 3(b)**). Garnet (<3%) occurred as euhedral crystals or as atoll including

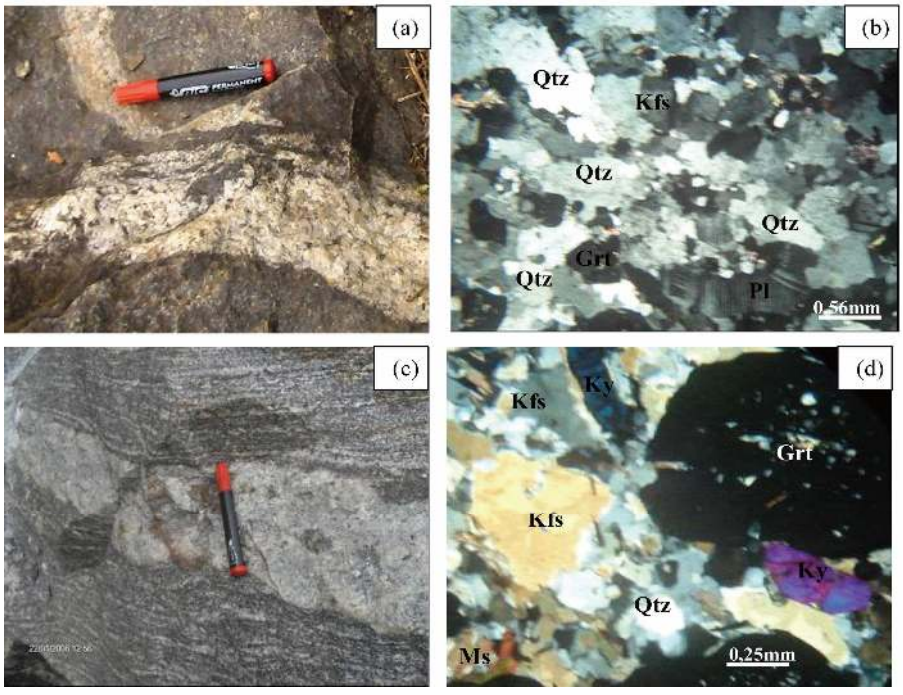

Figure 3. Field occurrences of injected leucosomes (a) and *in situ* leucosomes (c), and detail of microstructure of injected leucosomes (b) and *in situ* leucosomes (d).

muscovite, rutile, plagioclase and quartz. The average mineral composition of garnet is presented in **Table 1**. Garnet forms solid solution (**Figure 4**) of almandine (X_{Fe}: 0.63 - 0.68) rich in pyrope (X_{Mg}: 0.24 - 0.30) meanwhile kyanite (<2%) is prismatic, crackled crystals associated with garnet. Accessory minerals include apatite, zircon, monazite and rutile;

ii) coarse-grained, mainly composed of ribbons or interstitial quartz (25% - 40%), plagioclase, K-feldspar and biotite. Plagioclase (10% - 45%; An_{17}-An_{18}) occurs as euhedral antiperthitic crystals with deformed twins and sometimes as porphyroblasts with inclusions of quartz and biotite flakes. K-feldspar (10% - 50%) occurs as large crystals and is often perthitic (Or_{95} Ab_5-Or_{86} Ab_{14}). Biotite (<2%) is of magnesian composition (X_{Mg}: 0.62 - 0.67, **Table 2**; **Figure 5**) and occurs as flakes of various dimensions, most of which contain small inclusions of zircon and apatite. Accessories are monazite, zircon, apatite and often sillimanite, calcite, tourmaline and muscovite.

2) *In situ* leucosomes

In situ leucosomes are the most abundant in the Yaoundé series. They are observed in both metapelite and metabasite (**Figure 3(c)**), structured or not, medium to coarsed-grained, mainly composed of quartz, plagioclase, K-feldspar and garnet. Quartz (30% - 35%) forms elongated or interstitial crystals with undulatory extinction. Plagioclase (An_{21}-An_{24}; 20% - 60%) are anhedral and antiperthitic ($Or_{92}Ab_8$-$Or_{90}Ab_{10}$) crystal with polycrystalline almond shape. K-feldspar (10% - 20%) is

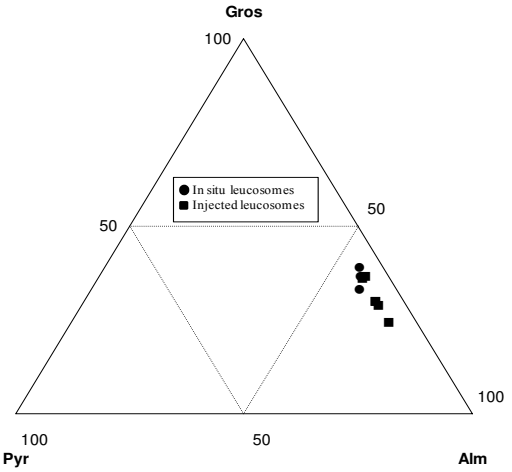

Figure 4. Triangular diagram showing the nature of garnet in Yaoundé leucosomes.

Table 1. Electron microprobe data of garnet from Yaoundé leucosomes.

Rocks	***In situ* leucosomes**			**Injected leucosomes**					
N°	3	16	19	6	7	8	15	16	17
SiO_2	39.31	39.50	38.70	39.25	38.36	38.32	37.80	38.88	38.67
Al_2O_3	22.82	22.96	22.74	22.85	22.77	23.00	23.31	22.65	22.81
FeO	27.31	26.93	25.46	28.27	30.06	28.54	28.81	26.16	27.03
MnO	0.69	0.79	0.50	0.61	0.86	0.50	0.52	0.77	0.50
MgO	8.58	9.70	10.19	7.50	5.98	7.44	7.70	9.23	9.46
CaO	2.88	2.26	1.96	1.85	2.01	2.20	1.89	2.06	2.29
TOTAL	101.58	101.14	99.55	100.33	100.04	100.00	100.03	99.75	100.76
Structural formula on the basis of 24 oxygens									
Si	5.956	5.936	5.924	6.031	5.975	5.933	5.860	5.966	5.902
Al	4.075	4.067	4.102	4.137	4.180	4.196	4.258	4.095	4.102
Fe	3.462	3.384	3.259	3.631	3.924	3.694	3.733	3.357	3.450
Mn	0.088	0.100	0.065	0.079	0.114	0.066	0.068	0.100	0.065
Mg	1.939	2.172	2.325	1.717	1.391	1.716	1.778	2.110	2.151
Ca	0.467	0.364	0.322	0.304	0.336	0.365	0.314	0.338	0.374
Alm (Fe)	0.58	0.56	0.55	0.64	0.63	0.68	0.63	0.57	0.57
Pyr (Mg)	0.33	0.36	0.39	0.29	0.30	0.24	0.30	0.36	0.36
Sp (Mn)	0.01	0.02	0.01	0.01	0.01	0.02	0.01	0.02	0.01
Gros (Ca)	0.08	0.06	0.05	0.06	0.06	0.06	0.06	0.05	0.06

Table 2. Electron microprobe data of biotite from Yaoundé leucosomes.

Rocks	*In situ* leucosomes						Injected leucosomes		
N°	44	45	47	48	49	50	35	36	37
SiO_2	38.03	37.70	37.65	38.16	38.04	37.71	37.61	38.20	37.22
Al_2O_3	18.28	18.04	18.48	18.24	17.69	18.48	17.38	17.30	17.64
FeO	12.39	12.12	12.00	11.49	12.17	11.96	11.59	1.61	11.45
MgO	13.19	13.22	12.71	12.92	13.16	13.13	13.59	13.59	13.42
K_2O	9.82	10.00	9.85	10.05	9.99	9.60	9.77	9.80	9.82
TiO_2	3.89	3.94	3.97	3.80	3.92	4.04	4.55	4.65	3.89
TOTAL	95.70	95.02	94.66	94.66	94.97	94.92	94.92	95.15	93.44
Structural formula on the basis of 22 oxygens									
Si	5.549	5.545	5.538	5.608	5.594	5.533	5.536	5.598	5.513
Al^{IV}	2.451	2.455	2.462	2.392	2.406	2.467	2.464	2.402	2.487
Al^{VI}	0.694	0.672	0.741	0.768	0.661	0.728	0.551	0.586	0.591
Fe	1.512	1.490	1.477	1.412	1.496	1.468	1.427	1.422	1.419
Mg	2.869	2.899	2.787	2.831	2.885	2.871	2.982	2.968	2.963
K	1.828	1.876	1.848	1.885	1.874	1.796	1.881	1.827	1.851
Ti	0.426	0.436	0.439	0.420	0.433	0.446	0.517	0.501	0.518
X_{Mg}	0.65	0.66	0.65	0.67	0.66	0.66	0.68	0.68	0.68

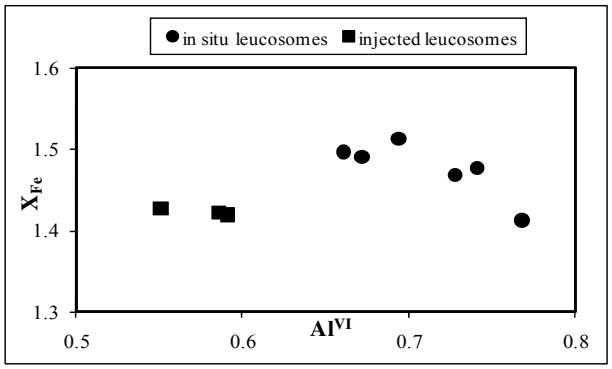

Figure 5. X_{Fe} vs Al^{VI} diagram showing the composition of biotite in Yaoundé leucosomes.

anhedral and perthitic ($Or_{89}Ab_{11}$-$Or_{93}Ab_7$). The perthitic composition ranges from $An_{18}Ab_{82}$ to $An_{20}Ab_{80}$. Garnets (<5%) appears as small euhedral crystals or zoned porphyroblasts (**Figure 3(d)**). The mineral composition of garnet is given in **Table 1**. They form a solid solution of almandine (X_{Fe}: 0.55 to 0.58) rich in pyrope (X_{Fe} = 0.33 to 0.39) and poor in spessartine (**Figure 4**). Biotite (≤3%) has magnesian composition (X_{Mg} = 0.65 - 0.67, **Table 2**) and appears as frayed flakes. Kyanite (<2%) is corroded twinned euhedral crystals (1 - 3 mm). They are often oriented or lodged between plagioclase, K-feldspar, garnet and quartz crystals (**Figure 3(d)**). Muscovite, monazite, zircon, rutile, apatite and oxides represent the accessory phase.

In the X_{Fe} vs Al^{VI} biotite diagram (**Figure 5**), there is a significant difference between *in situ* leucosomes and injected leucosomes. *In situ* leucosomes are enriched in both aluminium and iron, whereas injected leucosomes are depleted with respect to the same elements.

4.2. Geochemistry

1) Major elements

We use the $Na_2O + K_2O$ vs SiO_2 of Middlemost [43] for chemical classification of the different types of lecosomes. *In situ* leucosomes plot in granite while injected leucosomes plot in granite and quartz monzonite fields (**Figure 6**). The rocks are silica rich (with a SiO_2 content ranging from 64.66 to 80.35 wt%, **Table 1**) and show a variable content in total alkaline content ($3.53 \leq Na_2O + K_2O \leq 4.84\%$ for *in situ* leucosomes; $6.15 \leq Na_2O + K_2O \leq 9.21\%$ for injected leucosomes). This high alkaline content is also expressed by the K_2O/Na_2O ratios range from 0.49 to 0.59 in *in situ* leucosomes and from 0.51 to 3.72 in injected leucosomes. In the K_2O vs SiO_2 diagram, the *in situ* leucosomes plot in the calc-alkaline domain while the injected leucosomes show high K-calcalkaline

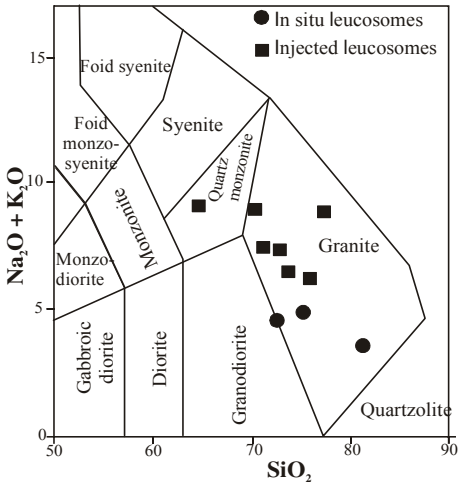

Figure 6. Classification diagram of plutonic rocks [43] showing the localization of the studied leucosomes in the granite field.

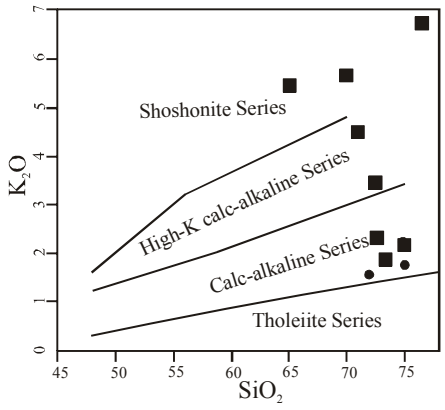

Figure 7. Diagram K_2O vs SiO_2 showing calc-alkaline, high-K to shoshonitic affinity of the Yaoundé leucosomes. Symbols as in Figure 6.

to shoshonitic affinities (**Figure 7**). In major elements variation diagrams vs SiO_2 (**Figure 8**), the two rock types form well defined clusters, and taken together define more or less well-defined trends. *In situ* leucosomes show decreasing concentration of K_2O, Al_2O_3, MgO, TiO_2 and CaO with an increase in SiO_2, while injected leucosomes show decreasing concentration of Al_2O_3, TiO_2, Fe_2O_3 and MgO with an increase in SiO_2. In the alumina index molar diagram ($Al_2O_3/(CaO + Na_2O + K_2O)$ vs $Al_2O_3/(Na_2O + K_2O)$), all the rocks plot in peraluminous field with *in situ* leucosomes conform to S-type and injected leucosomes conform to S-type and I-type granitoids (**Figure 9**).

2) Trace elements

Trace elements concentrations of the different leucosomes are listed in **Table 3**. Selected elements are plotted against SiO_2 in **Figure 10**. In *in situ* leucosomes, Rb and Zr concentrations decrease with increasing of SiO_2 while Y, Sr are scatter with increasing of SiO_2. In injected leucosomes Zr, Sr, Y contents decrease when SiO_2 contents increase (**Figure 10**). The K/Rb ratios (261 - 361 for *in situ* leucosomes; average at 315 and 351 - 737 for injected leucosomes; average at 480) are similar to those observed in the continental calc-alkaline igneous series [44,45]. Chondrite-normalized REE (the normalizing values are from Jahn *et al.* [29]) patterns show that the two types of leucosomes are much fractionated. *In situ* leucosomes have a strong LREE (Light Rare Earth Element) enrichment (Ce_N/Sm_N = 1.5 - 2.03) compared to HREE (GD_N/Yb_N = 1.20 - 1.54) with more pronounced positive Eu anomalies (Eu/Eu* = 1.29 - 1.36) for some and weakly negative Eu anomalies (Eu/Eu* = 0.93) for the others (**Figure 11(A)**). Injected leucosomes are also characterised by a strong HREE (heavy rare earth element) depletion (Gd_N/Yb_N = 1.60 - 16.20) and LREE enrichment (Ce_N/Sm_N = 2.19 - 4.70; **Figure 11(B)**). The REE patterns lead to the distinction of two groups of injected leucosomes: 1) a first group (**Figure 11(Ba)**) characterized by strong Eu positive anomalies (Eu/Eu* = 2.01 - 8.84) and, 2) a second group (**Figure 11(Bb)**) with negative to null Eu anomalies (Eu/Eu* = 0.63 - 1.22) and a strong enrichment in LREE (Ce_N/Sm_N = 2.19 - 4.70). These geochemistry behaviours are in accordance with subdivisions done in petrography.

4.3. Geochronology

4.3.1. U-Th-Pb Age on Monazite

Two samples of leucosomes (OL3A & OL3B) were selected for U-Th-Pb monazite ages. These samples were chosen because they are more enriched in monazite crystals than other samples. The analyzed monazite crystals are of two main types: 1) globular or ovoid crystals, often crackled with no optical zoning (**Figures 12(a)** and **(b)**); 2) prismatic crystals, also with no optical zoning, but spotted by opaque granules which form inclusions in biotite flakes (**Figures 12(b)** and **(c)**). No systematic core-to-rim optical age zonation of were observed. This observation implies that monazite crystallize from melting liquid. This allows the calculation of ages composed of several single analyses by regression through zero [34] and of weighted means [41]. Chemical Th-U-Pb ages (**Tables 4** and **5**) have been gotten by Electron microprobe analysis (EMP). Two groups of ages, corresponding probably to the two events of monazite crystallisation, are recognised in the diagrams of mineral chemistry of monazite element vs Th-U-Pb chemical ages (**Figures 13** and **14**). The first event (younger) occurs at around 600 Ma and the second (older) at around 660 Ma. The analysed monazite age data are compared in the PbO vs ThO_2* diagram (**Figure 15(a)**) of Suzuki *et al.* [46]. On this diagram, the two generations of monazite previously described are clearly individualized. The average age of

Table 3. Representative major (wt%) and traces (ppm) elements analyses of the Yaoundé leucosomes.

Samples	*In situ* leucosomes						Injected leucosomes							
							Fine grained			Coarse grained				
	OL8b	16b	MB13b	MM86L	A16L	OL8L	MM14	MB2a	MM20b	OL14	MM2	MM10	MS20b	OL11
SiO_2	72.03	74.66	80.35	72.73	74.7	72.03	64.66	69.57	72.1	70.79	72.77	73.01	75.54	77.22
Al_2O_3	13.07	11.97	8.62	15.06	12	13.07	18.24	16.47	15.63	15.38	16.18	15.98	14.78	12.08
Fe_2O_3	4.74	3.48	3.7	2.4	2.48	4.74	2.16	0.83	1.36	2.45	0.62	0.8	0.48	0.51
MnO	0.06	0.06	0.05	0.06	0.06	0.06	0.05	0.01	0.01	0.04	0.02	0.03	0.01	0.02
MgO	2.17	1.73	1.04	0.7	1.73	2.17	0.78	0.43	0.52	0.98	-	0.03	0.27	0.02
CaO	1.91	2	1.24	2.1	2	1.91	3.04	2.25	1.95	1.96	2.68	2.57	2.14	0.39
Na_2O	2.86	3.1	2.01	3.56	3.1	2.86	3.93	3.49	3.88	3.5	4.28	3.84	3.79	1.87
K_2O	1.7	1.74	1.52	1.73	1.74	1.7	5.18	5.41	3.37	3.92	2.17	2.55	2.36	6.97
TiO_2	0.7	0.52	0.41	0.3	0.52	0.7	0.35	0.27	0.21	0.31	0.08	0.12	0.11	0.7
P_2O_5	-	-	-	0.06	-	-	-	-	0.02	-	-	-	-	-
LOI	0.61	0.51	0.56	1.16	0.51	0.61	0.7	0.98	0.51	0.38	0.47	0.54	0.22	0.43
Rb	54	40	39	33	40	54	107	123	38	93	29	36	46	165
Sr	193	211	121	379	211	193	660	391	469	315	398	380	386	286
Zr	185	135	83	75	135	135	164	99	97	80	41	91	40	18
Nb	4	4	6		4	4	-	-	-	3	-	-	-	2
Y	25	22	24	10	22	22	15	11	18	16	10	11	10	9
La	12.22	15.85	21	21.03	15.9	12.22	67.38	40.68	41.12	20.6	6.34	7.12	4.09	9.43
Ce	24.53	31.91	44.27	41.91	31.9	24.53	142.71	79.36	79.58	40.59	10.48	12.79	6.51	14.96
Nd	13.91	14.17	21.16	15.46	14.2	13.91	73.07	34.15	36.41	20.58	3.27	4.05	1.87	6.7
Sm	3.75	3.39	4.57	3.18	3.39	3.75	15.38	6.17	7.31	4.31	0.64	0.71	0.33	1.31
Eu	1.55	1.47	1.26	2.36	1.47	1.55	2.83	2.14	1.37	2.33	1.48	1.64	0.79	2.26
Gd	3.54	3.17	3.59	2.64	3.17	3.54	11.49	4.48	6.35	2.97	0.53	0.77	0.23	0.88
Dy	3.34	2.85	3.29	2.03	2.85	3.34	3.36	1.55	6.02	2.09	0.39	0.5	0.1	0.41
Er	1.98	1.57	1.96	1.24	1.57	1.98	0.99	0.49	0.37	1.15	0.2	0.38	0.05	0.23
Yb	2.17	1.65	2.41	1.25	1.65	2.17	0.57	0.26	0.35	1.12	0.17	0.38	0.05	0.16
Lu	0.3	0.32	0.38	0.2	0.32	0.3	0.13	0.05	0.12	0.17	0.06	0.05	0.01	0.06
K/Rb	261	361	324	-	-	-	402	365	737	351	621	588	426	351
Rb/Sr	0.28	0.19	0.32	-	-	-	0.16	0.31	0.08	0.3	0.07	0.09	0.12	0.58
Ca/Sr	70.7	67.68	73.17	-	-	-	32.89	41.09	29.4	44.43	48.08	48.29	39.58	9.74
(Ce/Sm)N	1.5	2.2	2.3	3.11	2.2	1.5	2.19	3.03	2.57	2.22	3.85	4.25	4.7	2.7
(Gd/Yb)N	1.3	1.54	1.2	1.7	1.54	1.3	16.2	13.84	14.6	2.13	2.5	1.6	3.7	4.4
(Ce/Yb)N	2.89	4.95	4.2	8.57	4.95	2.89	64.06	78.1	58.3	9.28	15.72	8.59	33.4	23.9
Eu/Eu*	1.29	1.36	0.93	2.44	1.36	1.29	0.63	1.22	0.64	2.01	7.8	6.65	8.84	6.12

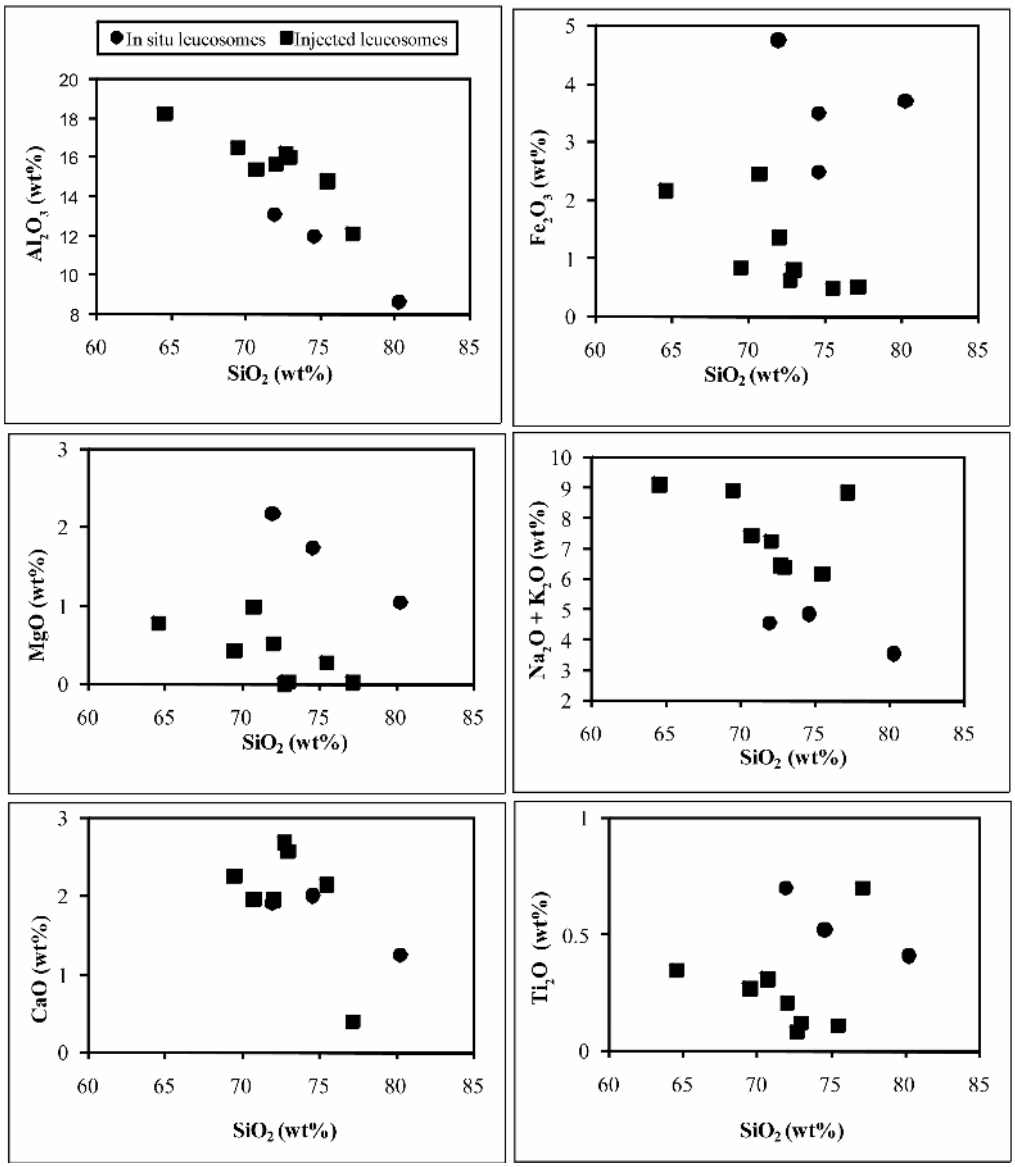

Figure 8. Harker diagrams of selected major elements. Symbols as in Figure 6.

the younger generation gives 592 ± 10 Ma while it gives 658 ± 25 Ma for the older one (**Figure 15(b)**). These two groups of ages seem to belong to the same thermal event because the petrography study reveals that all the monazite crystals are included in biotite flakes. Statistically, all these data can be considered as belonging to the same crystal population.

4.3.2. LA-ICP-MS U-Pb Zircon Ages

1) U-Pb zircon ages of leucosomes

Fourteen grains of zircons from the leucosomes of metapelite were analyzed by the LA-ICP-MS method (**Table 6**). The Concordia diagrams (**Figure 16**) obtained reveal a concordant Pan-African age at 626 ± 6.4 Ma (MSWD = 2.1). The analyzed zircons crystals did not show any sign of a complex history. The obtained concordant ages correspond to the melting age during the Pan-African orogeny in Cameroon.

For the leucosomes occurring in metabasite, sixteen grains of zircons were analyzed by the same method. The obtained results (**Table 7**) define a Discordia (**Figure 17**) with an average Pan-African age at 654 ± 6.7 Ma (MSWD = 1.3).

2) U-Pb zircon age of metapelitic (basement)

Two types of zircon crystals (zoned and no zoned) were identified in metasediment. Zoned zircon crystals are observed in the leucosomes from the metasediment whereas no zoned zircon crystals were selected from paleosome. The analytical results of no zoned zircons are listed on **Table 8**. The ages obtained define a Discordia

Table 4. Electron microprobe analyses of monazite from Yaoundé leucosomes (sample OL3A). Monazite ages from single analyses are given with minimal error (see text).

Sample	OL3A																	
No	SiO_2	Al_2O_3	P_2O_5	CaO	La_2O_3	Ce_2O_3	Pr_2O_3	Sm_2O_3	Nd_2O_3	Eu_2O_3	Gd_2O_3	ThO_2	UO_2	PbO	SrO	Y_2O_3	Total	Age
Madmon	2.33	0.00	24.79	0.16	7.10	24.15	3.72	5.15	16.17	0.00	2.58	13.82	0.54	0.33	0.00	1.41	102.25	**489**
7	0.25	0.03	30.65	1.05	14.12	28.94	3.00	1.88	12.48	0.82	1.18	4.25	0.47	0.15	0.13	0.77	100.17	577
36	0.25	0.01	30.16	1.31	14.29	28.80	2.91	2.00	12.01	0.64	1.08	5.60	0.51	0.19	0.12	0.11	99.98	612
37	0.23	0.00	30.08	1.30	14.39	28.80	2.83	1.96	11.74	0.64	1.06	5.51	0.50	0.19	0.13	0.11	99.47	631
38	0.38	0.02	29.77	1.37	13.75	28.70	3.03	1.76	12.32	0.64	0.78	6.23	0.35	0.18	0.14	0.04	99.43	565
39	0.40	0.02	29.85	1.34	13.78	28.56	3.04	1.81	12.62	0.62	0.75	6.19	0.34	0.18	0.14	0.01	99.65	588
41	0.21	0.00	30.14	1.19	14.85	29.15	2.94	1.96	12.01	0.63	1.02	4.99	0.48	0.14	0.14	0.12	99.97	513
65	0.80	0.15	29.24	1.35	14.44	28.48	3.01	1.81	11.91	0.73	0.94	5.19	0.69	0.20	0.14	0.14	99.20	615
66	0.33	0.03	30.15	1.35	14.78	28.84	2.89	1.88	11.55	0.78	0.88	5.42	0.89	0.20	0.15	0.07	100.18	561
68	0.37	0.02	30.03	1.13	13.87	27.98	2.69	2.10	11.30	0.89	1.49	4.88	0.76	0.18	0.14	0.94	98.74	561
69	0.35	0.03	29.32	1.42	14.57	28.31	2.98	1.96	11.77	0.79	0.90	5.74	0.94	0.22	0.14	0.06	99.50	599
70	0.37	0.03	30.19	1.30	14.49	28.78	2.94	1.92	11.81	0.73	0.99	5.33	0.67	0.19	0.14	0.06	99.92	586
5	0.26	0.02	29.28	0.69	14.18	29.60	3.23	1.83	13.02	0.91	1.20	3.10	0.36	0.13	0.15	0.71	98.66	667
6	0.21	0.01	30.57	0.80	13.86	28.91	3.00	1.96	12.19	0.97	1.35	3.10	0.41	0.13	0.14	1.34	98.93	651
35	0.27	0.01	30.14	1.35	14.20	28.59	2.86	1.95	11.76	0.66	1.09	5.76	0.52	0.22	0.15	0.10	99.62	689
42	0.35	0.01	30.07	1.38	13.79	28.77	3.00	1.86	12.51	0.61	0.75	6.19	0.37	0.20	0.14	0.05	100.04	650
71	0.37	0.01	29.69	1.32	13.96	27.96	2.97	1.97	11.86	0.80	1.24	5.51	0.77	0.23	0.14	0.59	99.38	667

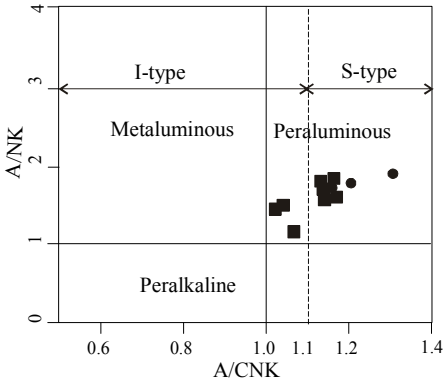

Figure 9. Molar A/NK vs A/CNK diagram showing the peraluminous character of Yaoundé leucosomes. Symbols as in Figure 6.

with upper intercept at 2127 ± 150 Ma and the lower intercept at 911 ± 56 Ma (**Figures 18(a)** and **(b)**). This means that the metapelitic rocks (*in situ* leucosomes rich) of the Yaoundé series underwent Paleoproterozoic history (2127 ± 150 Ma) before the overprinting of an early Pan-African event at around 911 Ma.

Zoned zircon crystals were also analyzed and their radiometric results are given in **Table 9**. The histogram (**Figure 19(a)**) of zoned zircon crystals shows two groups of ages. This is confirmed in the Discordia diagram (**Figure 19(b)**) where the ages are discordant and define two intercepts with upper intercept at 1122 ± 110 Ma and the lower one at 620 ± 61 Ma. The 1122 Ma age of the upper intercept confirms the existence within the Yaoundé series of a metamorphic event between 1122 Ma and 911 Ma as revealed by radiometric data of no zoned zircon from metapelite. The lower intercept age (620 ± 61 Ma) is similar to the age previously obtained on no zoned zircons of metapelitic rock (626 ± 6 Ma; **Figure 16**) and probably corresponds to the melting age. The Tonien-Stenien event (911 - 1122 Ma) is new in the Yaoundé series and in the Pan-African North-Equatorial Fold Belt in general. This period can be interpreted as the beginning of metamorphism in the Yaoundé series.

5. Discussion

5.1. Origin and Petrogenesis of Leucosomes in the Yaoundé Series

Peraluminous magmatism is commonly associated to the

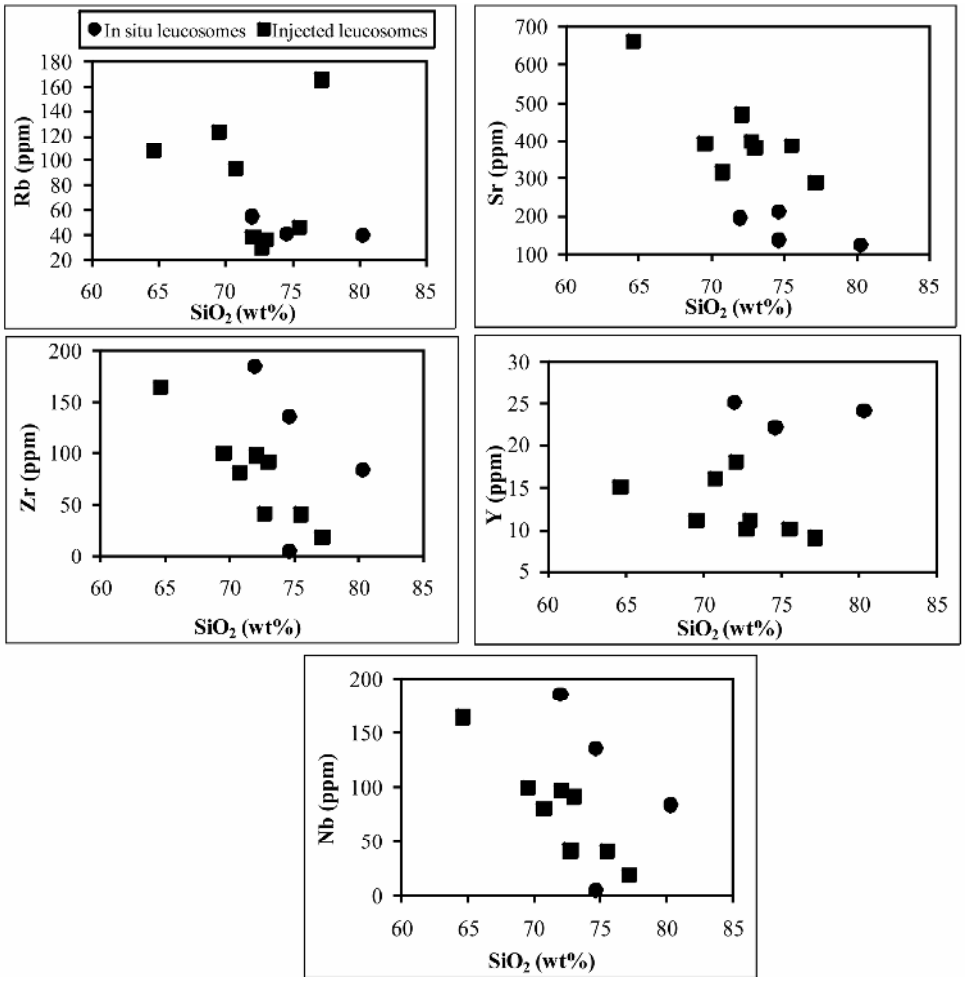

Figure 10. Harker diagrams of selected trace elements. Symbols as in Figure 6.

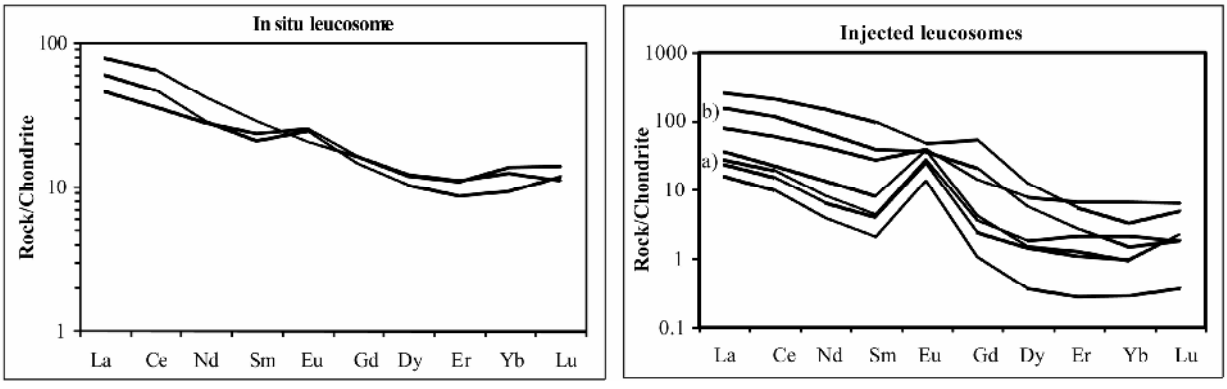

(a) (b)

Figure 11. Chondrite-normalized REE patterns (the normalising values are from Jahn *et al.*, 1978) for *in situ* leucosomes (a) and injected leucosomes (b).

deformed and metamorphosed rocks of the orogenic belt (along faults and shear zones) or occurs as syn to post-tectonic plutons [47-49]. Three main models have been proposed to explain the formation of peraluminous granitoids: 1) partial melting of quartzo-feldspathic orthogneisses [50]; 2) reaction between basaltic melts and crustal rocks [51]; and 3) the spatial association and the presence of metasedimentary enclaves in the leucogranites suggesting an origin from partial melts of metasedimentary rocks [13,52,53].

Table 5. Electron microprobe analyses of monazite from Yaoundé leucosomes (sample OL3B). Monazite ages from single analyses are given with minimal error (see text).

Sample	OL3B																	
No	SiO_2	Al_2O_3	P_2O_5	CaO	La_2O_3	Ce_2O_3	Pr_2O_3	Sm_2O_3	Nd_2O_3	Eu_2O_3	Gd_2O_3	ThO_2	UO_2	PbO	SrO	Y_2O_3	Total	Age
Madmon	2.33	0.00	24.79	0.16	7.10	24.15	3.72	5.15	16.17	0.00	2.58	13.82	0.54	0.33	0.00	1.41	102.25	**489**
8	0.41	0.01	30.37	1.35	14.04	29.25	2.92	1.79	11.85	0.60	0.62	6.36	0.31	0.18	0.13	0.01	100.17	559
9	0.28	0.00	30.38	1.31	14.51	29.11	2.86	2.05	11.79	0.68	1.05	5.04	0.83	0.19	0.16	0.34	100.56	565
10	0.31	0.00	29.93	1.34	14.44	28.92	3.08	1.95	12.08	0.65	0.94	5.48	0.67	0.20	0.15	0.23	100.34	596
11	0.32	0.00	29.98	1.35	13.89	29.41	3.04	1.91	12.36	0.59	0.71	6.03	0.34	0.19	0.13	0.01	100.26	631
12	0.42	0.00	29.83	1.43	13.87	29.07	2.84	1.86	11.69	0.52	0.70	6.63	0.37	0.20	0.14	0.04	99.61	590
13	0.46	0.03	29.19	1.41	13.74	28.94	3.28	1.91	13.00	0.58	0.70	6.48	0.35	0.18	0.14	0.01	100.41	563
15	0.46	0.01	30.05	1.35	14.13	29.16	3.11	1.81	12.45	0.62	0.60	6.16	0.29	0.17	0.15	0.01	100.51	550
17	0.59	0.16	29.39	1.38	14.00	28.02	3.07	1.95	12.27	0.64	1.04	5.36	0.43	0.17	0.15	0.07	98.70	602
18	0.28	0.05	30.08	1.23	14.37	28.62	2.94	1.84	11.34	0.66	0.99	5.41	0.40	0.17	0.16	0.13	98.64	600
19	0.33	0.05	29.78	1.28	14.37	28.53	2.81	1.94	11.06	0.69	1.09	5.43	0.59	0.19	0.14	0.31	98.57	597
20	0.32	0.11	30.41	1.25	14.48	28.93	3.13	1.96	12.20	0.68	0.96	5.24	0.45	0.18	0.15	0.09	100.54	613
21	0.26	0.05	26.43	0.94	8.92	19.45	2.07	1.13	7.59	0.42	0.54	3.99	0.33	0.13	0.12	0.10	72.47	607
22	0.29	0.06	25.35	1.01	10.55	19.23	2.07	1.17	7.94	0.50	0.57	4.20	0.81	0.17	0.15	0.05	74.12	565
23	0.26	0.09	30.18	0.83	16.22	30.10	3.00	1.82	11.79	0.67	1.10	2.44	0.77	0.13	0.15	0.16	99.72	615
24	0.33	0.05	29.92	1.29	14.11	28.29	2.91	2.02	11.98	0.70	1.03	5.52	0.50	0.18	0.15	0.06	99.02	605
25	0.32	0.03	29.84	1.28	14.28	28.69	2.79	1.95	11.52	0.65	1.06	5.53	0.47	0.17	0.13	0.08	98.81	572
26	0.33	0.02	30.37	1.40	14.25	28.50	3.02	1.89	12.46	0.67	1.05	5.96	0.50	0.20	0.13	0.07	100.82	611
27	0.27	0.01	30.13	1.38	14.25	28.66	2.88	1.84	11.56	0.62	1.01	6.00	0.49	0.20	0.13	0.07	99.48	606
28	0.32	0.02	29.69	1.39	14.27	28.43	2.91	1.88	11.67	0.65	1.01	6.08	0.50	0.19	0.14	0.09	99.21	579
29	0.26	0.02	25.10	1.04	10.06	19.37	2.04	1.15	7.56	0.42	0.61	4.83	0.39	0.15	0.14	0.06	73.18	576
30	0.41	0.04	28.57	1.39	14.21	28.43	3.04	1.83	12.35	0.69	1.06	6.06	0.49	0.20	0.16	0.11	99.05	615
31	0.29	0.02	29.98	1.37	14.60	28.91	2.93	1.83	11.82	0.66	1.01	5.66	0.48	0.19	0.16	0.10	100.00	616
32	0.33	0.03	30.05	1.28	14.40	28.94	3.07	1.74	12.05	0.64	1.01	5.59	0.42	0.17	0.14	0.10	99.95	573
33	0.33	0.01	29.83	1.40	14.34	28.77	3.01	1.78	11.51	0.65	1.01	6.07	0.50	0.20	0.15	0.09	99.65	596
43	0.40	0.02	30.35	1.28	14.31	29.40	2.93	1.64	11.71	0.63	0.76	5.65	0.38	0.18	0.12	0.05	99.82	628
45	0.35	0.01	30.25	1.25	14.14	29.54	2.99	1.83	12.24	0.63	0.75	5.50	0.39	0.18	0.14	0.02	100.20	609
47	0.37	0.02	30.53	1.28	14.23	29.22	2.93	1.73	11.93	0.64	0.96	5.35	0.69	0.20	0.12	0.13	100.32	602
48	0.30	0.11	29.94	1.19	14.37	29.04	3.03	1.97	11.83	0.67	0.97	5.09	0.43	0.16	0.14	0.10	99.35	594
50	0.28	0.07	29.99	1.24	14.66	29.05	2.91	1.98	11.80	0.78	0.97	5.12	0.68	0.19	0.15	0.25	100.10	608
82	0.29	0.01	30.38	1.24	14.37	28.64	3.06	1.91	12.33	0.77	1.14	4.73	0.79	0.18	0.14	0.57	100.55	581
52	0.29	0.10	29.96	1.24	14.41	29.18	3.19	1.96	12.27	0.64	0.90	5.37	0.38	0.17	0.14	0.05	100.23	615
73	0.29	0.03	30.17	1.27	14.29	28.44	2.91	1.79	11.84	0.76	1.09	4.97	0.84	0.19	0.16	0.57	99.61	578
74	0.20	0.01	29.74	0.64	14.90	29.46	3.03	1.99	11.62	0.89	1.44	2.31	0.71	0.13	0.15	0.69	97.89	638
75	0.33	0.02	29.84	1.41	14.46	28.00	3.00	1.86	11.59	0.81	0.98	6.03	0.90	0.22	0.16	0.26	99.85	572
76	0.21	0.00	30.13	0.75	14.51	29.50	3.13	1.96	12.04	0.94	1.34	2.81	0.86	0.14	0.15	0.72	99.19	574
77	0.35	0.00	29.88	1.41	14.42	28.00	2.73	1.86	11.38	0.80	0.92	5.71	0.94	0.22	0.15	0.15	98.91	585
79	0.22	0.00	30.41	0.70	14.81	29.01	3.04	1.92	11.96	0.88	1.30	2.54	0.94	0.14	0.14	0.88	98.87	569
81	0.26	0.02	30.58	1.22	14.54	28.61	3.12	1.85	12.10	0.78	1.17	4.84	0.82	0.20	0.13	0.57	100.80	612
49	0.33	0.10	28.34	1.24	14.65	28.40	2.96	1.80	11.96	0.69	0.99	5.14	0.68	0.20	0.17	0.42	98.06	625
51	0.35	0.11	29.19	1.27	14.40	29.07	2.93	1.77	12.47	0.66	0.73	5.66	0.31	0.18	0.14	0.03	99.26	639
16	0.32	0.00	29.97	1.31	14.24	29.01	3.14	2.04	12.72	0.63	1.00	5.68	0.37	0.19	0.15	0.02	100.79	644
34	0.29	0.01	24.58	0.95	9.62	20.90	2.22	0.92	8.61	0.47	0.75	4.94	0.30	0.16	0.16	0.09	74.98	645
42	0.35	0.01	30.07	1.38	13.79	28.77	3.00	1.86	12.51	0.61	0.75	6.19	0.37	0.20	0.14	0.05	100.04	650
44	0.38	0.02	30.15	1.27	14.27	29.58	2.93	1.67	11.81	0.61	0.72	5.71	0.37	0.19	0.14	0.04	99.87	661
78	0.36	0.01	29.95	1.19	14.28	28.34	3.06	1.88	11.68	0.69	1.31	5.15	0.52	0.19	0.14	0.51	99.26	645

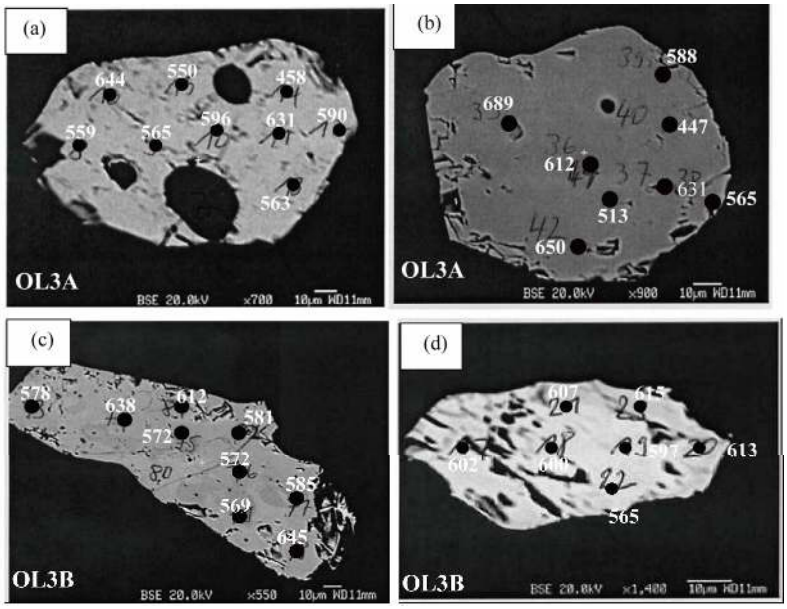

Figure 12. Backscattered electron images of selected dated monazite crystals in Yaoundé leucosomes: (a) and (b) Globular shape crystals; (c) and (d) Prismatic crystals.

Table 6. LA-ICP-MS U-Pb results for zircons from leucosomes in metapelite of the Yaoundé series.

Sample	Isotopic ratios						Apparent ages						rho
	$^{207}Pb/^{206}Pb$	%2σ	$^{207}Pb/^{205}U$	2σ	$^{206}Pb/^{208}U$	2σ	$^{207}Pb/^{206}Pb$	2σ	$^{207}Pb/^{205}U$	2σ	$^{206}Pb/^{208}U$	2σ	
Z6	0.0605	0.8766	0.8432	3.19	0.1011	3.07	620.9815	18.91	620.8974	14.82	620.8744	18.16	0.96
Z9	0.0647	1.0745	1.0648	2.08	0.1194	1.78	763.8462	22.64	736.1893	10.87	727.1329	12.22	0.86
Z11	0.0602	0.8210	0.9097	1.95	0.1096	1.77	610.7711	17.74	656.8983	9.44	670.4097	11.27	0.91
Z14	0.0615	0.9516	0.8467	2.26	0.0998	2.04	657.5927	20.41	622.8499	10.50	613.3286	11.96	0.91
Z16	0.0597	1.0440	0.8588	2.07	0.1044	1.79	592.0281	22.63	629.4851	9.72	639.9615	10.90	0.86
Z18	0.0599	1.3962	0.9419	2.61	0.1141	2.20	599.6740	30.23	673.8698	12.85	696.2775	14.55	0.84
Z23	0.0598	1.1160	0.8539	3.77	0.1036	3.61	595.9765	24.18	626.8027	17.65	635.3784	21.82	0.96
Z27	0.0602	0.8331	0.8535	3.09	0.1029	2.98	609.2004	18.01	626.5621	14.46	631.3819	17.91	0.96
Z28	0.0601	0.9413	0.9017	3.86	0.1087	3.75	608.8288	20.35	652.6611	18.59	665.4089	23.68	0.97
Z29	0.0604	1.1882	0.8103	2.50	0.0973	2.19	618.0647	25.65	602.6232	11.34	598.5263	12.54	0.88
Z31	0.0600	5.5132	0.8380	3.95	0.1013	3.49	603.6146	115.02	618.0268	12.31	621.9688	20.77	0.88
Z33	0.0578	3.2449	0.8111	2.45	0.1017	1.69	523.8707	69.62	603.0479	6.46	624.3219	10.14	0.69
Z37	0.0602	1.0918	0.8647	3.04	0.1042	2.83	609.3628	23.60	632.6981	14.29	639.2483	17.23	0.93
Z38	0.0593	3.7630	0.8331	2.70	0.1019	2.16	577.5185	79.74	615.3266	7.25	625.6504	12.97	0.80

The leucosomes of the Yaoundé series are characterized by: 1) their peraluminous affinity; 2) their Rb/Zr weak ratios (0.2 - 6.38) characteristic of granites of crustal origin [54]; 3) the relative low content in Sr (1.93 - 499), the relative enrichment in K_2O (1.52 - 5.18) and the relatively low contents in CaO (1.24 - 3.04) characteristic of the rocks of pelitic origin [55]. Their chemical composition is similar to S-type granite from S-type Transamazonian and Hercynian peraluminous leucogranites [55, 56] and to that of melts produced experimentally from sedimentary protoliths [57,58]. The enrichment in alkali in relation with CaO is characteristic of calc-alkaline Cordillera type granitoids [59]. In molar diagram CaO/(MgO + FeOt) vs Al_2O_3/(MgO + FeOt) of Altherr

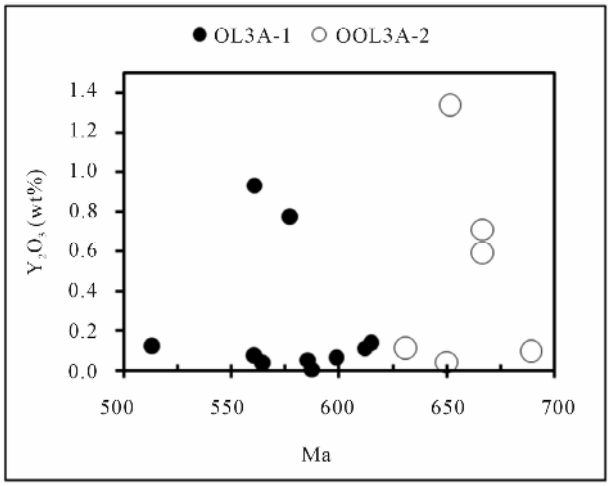

(a)

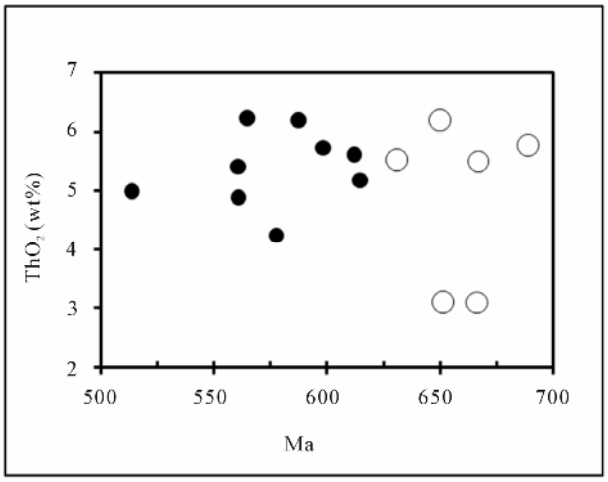

(b)

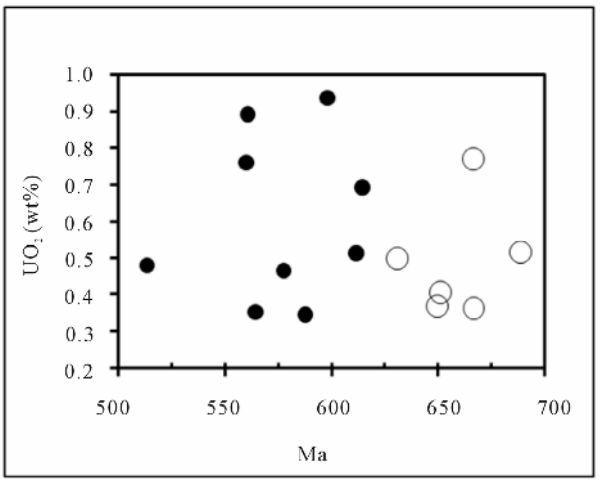

(c)

Figure 13. Mineral chemistry of monazites vs Th-U-Pb chemical ages of sample OL3A. (a) Y_2O_3 of monazites vs age; (b) ThO_2 of monazite vs age; (c) UO_2 of monazites vs age.

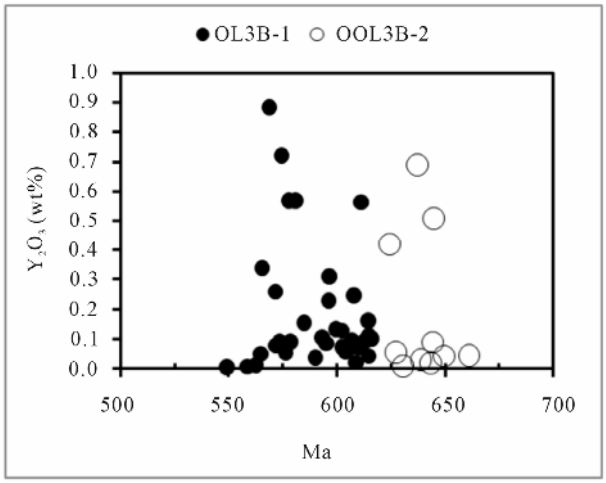

(a)

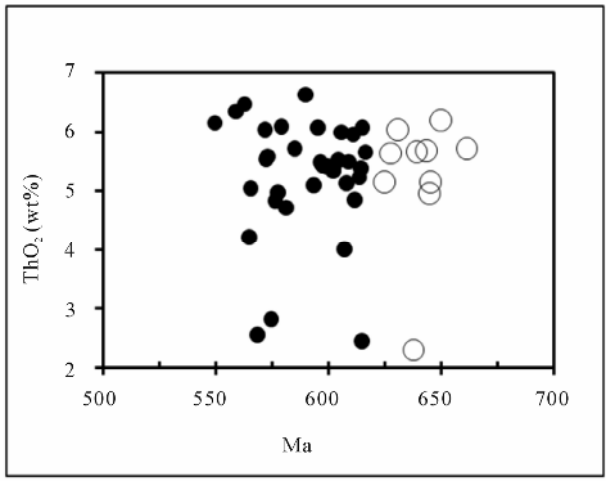

(b)

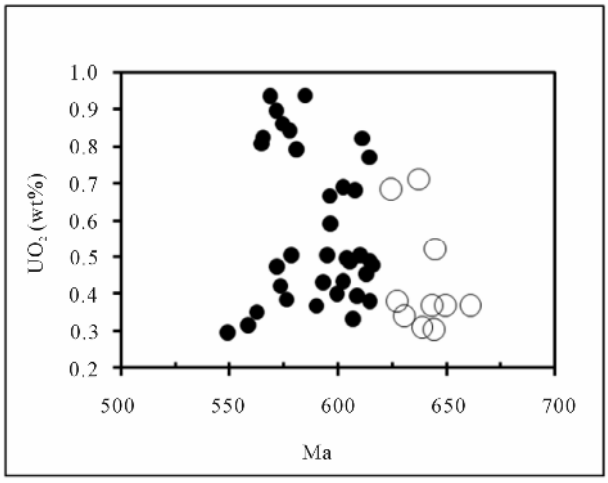

(c)

Figure 14. Mineral chemistry of monazites vs Th-U-Pb chemical ages of sample OL3B. (a) Y_2O_3 of monazites vs age; (b) ThO_2 of monazite vs age; (c) UO_2 of monazites vs age.

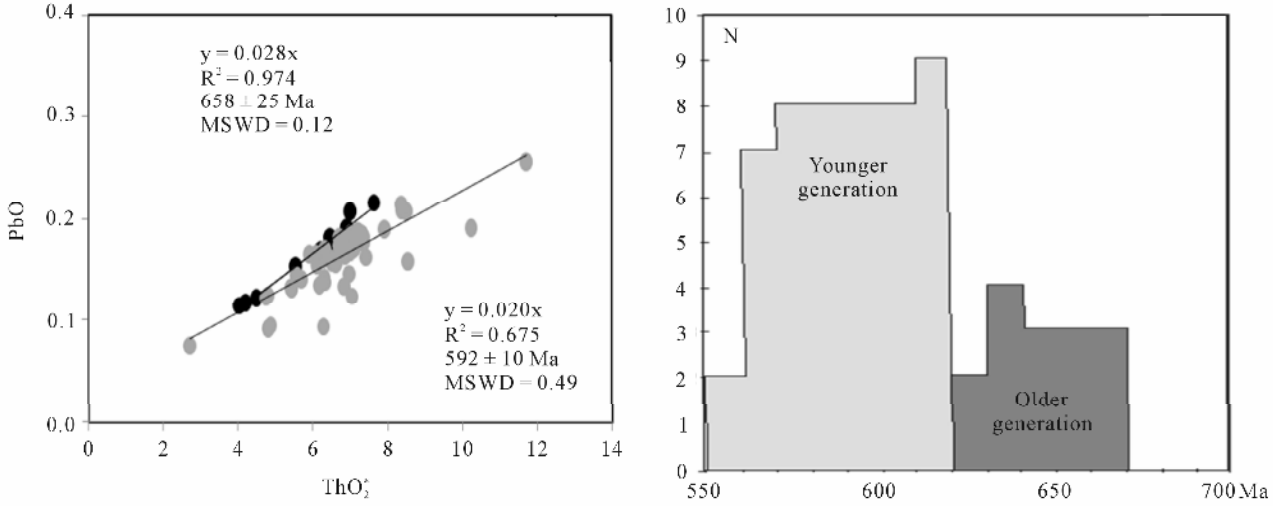

(a) (b)

Figure 15. (a) Th-U-Pb CHIME model ages for Yaoundé leucosomes. Total PbO vs ThO_2^* (wt%) isochron diagram; ThO_2^* = ThO_2 + UO_2 equivalents expressed as ThO_2, after [46]. Isochron age derived from these diagrams broadly match weighted average ages calculated for the rocks according to [34]; (b) Histogram view of EMP-Th-U-Pb monazite ages.

Table 7. LA-ICP-MS U-Pb results for zircons from leucosomes in metabasite of the Yaoundé series.

Sample	Isotopic ratios						Apparent ages					
	$^{207}Pb/^{206}Pb$	2σ	$^{207}Pb/^{205}U$	2σ	$^{206}Pb/^{208}U$	2σ	$^{207}Pb/^{206}Pb$	2σ	$^{207}Pb/^{205}U$	2σ	$^{206}Pb/^{208}U$	2σ
Z1	0.0619	0.99	0.7891	2.18	0.0924	1.95	671.1023	21.19	590.6603	9.78	569.9372	10.61
Z2	0.0613	0.95	0.8539	2.12	0.1009	1.89	651.3840	20.50	626.7634	9.92	619.9625	11.19
Z2 nuc	0.0616	0.97	0.8047	2.17	0.0947	1.94	660.5042	20.81	599.4976	9.82	583.4934	10.82
Z3	0.0624	1.64	0.8284	3.68	0.0962	3.29	689.4344	35.00	612.6979	16.91	592.1415	18.61
Z4	0.0615	1.03	0.8250	2.43	0.0972	2.20	657.8133	22.09	610.8348	11.16	598.2421	12.58
Z5	0.0617	0.79	0.8257	1.94	0.0971	1.77	663.6617	16.94	611.2062	8.89	597.1463	10.08
Z6	0.0627	0.72	0.8322	1.82	0.0962	1.68	699.7667	15.28	614.8545	8.41	592.0477	9.48
Z7	0.0613	1.66	0.8491	3.84	0.1005	3.46	649.7675	35.65	624.1353	17.91	617.0873	20.38
Z8	0.0605	0.89	0.8205	1.91	0.0984	1.69	620.1877	19.29	608.3527	8.74	605.1796	9.74
Z9	0.0613	1.00	0.8383	2.23	0.0991	1.99	651.4618	21.54	618.2209	10.31	609.1809	11.56
Z10	0.0610	0.70	0.8326	1.63	0.0990	1.47	638.4511	15.04	615.0440	7.51	608.7049	8.54
Z11	0.0612	1.39	0.7908	3.18	0.0938	2.86	644.7045	29.90	591.6114	14.27	577.8623	15.82
Z12	0.0617	0.89	0.8647	1.90	0.1016	1.68	663.8725	19.06	632.7046	8.96	624.0163	10.00
Z13	0.0622	0.70	0.8577	1.49	0.1000	1.31	681.9553	15.01	628.8560	6.96	614.1906	7.66
Z16	0.0611	0.65	0.8468	1.40	0.1005	1.23	642.4081	14.03	622.8909	6.50	617.5314	7.26
Z17	0.0607	1.95	0.8335	4.34	0.0996	3.87	629.0979	42.02	615.5313	20.02	611.8495	22.61

et al. [60], the *in situ* leucosomes are plotted in the field of partial melts from metapelite source whereas the injected leucosomes are plotted in the field of partial melt from metagreywacke source (**Figure 20**). These sources, which are predominantly found in the upper part of the continental crust, allow us to confirm that the source of *in situ* leucosomes was the metapelitic host rocks and to suggest that the injected leucosomes are originated

Table 8. LA-ICP-MS U-Pb results for no zoned zircons from leucosomes in metapelite of the Yaoundé series.

Sample	Isotopic ratios						Apparent ages						rho
	$^{207}Pb/^{206}Pb$	%2σ	$^{207}Pb/^{205}U$	2σ	$^{206}Pb/^{208}U$	2σ	$^{207}Pb/^{206}Pb$	2σ	$^{207}Pb/^{205}U$	2σ	$^{206}Pb/^{208}U$	2σ	
Z1	0.1200	0.99	5.1092	3.73	0.3088	3.6	1955.922	17.64	1837.6284	31.68	1735.0134	54.73	0.96
Z2	0.0674	1.37	1.2642	2.56	0.1360	2.17	850.7457	28.38	829.7947	14.52	821.9938	16.71	0.85
Z5	0.0717	1.43	1.4640	3.14	0.1481	2.79	977.7781	29.07	915.6620	18.92	890.1041	23.23	0.89
UQZ	0.0787	1.16	2.1010	2.28	0.1936	1.97	1164.735	22.89	1149.1404	15.7	1140.8935	20.57	0.86
Z10	0.0749	1.42	1.6876	2.46	0.1634	2.01	1066.207	28.5	1003.8718	15.67	975.5618	18.17	0.82
Z13	0.0616	5.10	1.1773	3.68	0.1387	3.17	659.0272	105.7	790.0483	11.03	837.2553	24.98	0.86
Z15	0.0719	1.16	1.5949	5.18	0.1608	5.05	983.6733	23.53	968.2228	32.32	961.4305	45.09	0.97
Z17	0.0723	0.86	1.6499	1.7	0.1654	1.47	995.2298	17.48	989.5054	10.78	986.9260	13.47	0.86
Z19	0.0768	1.37	1.8392	3.69	0.1737	3.42	1115.352	27.33	1059.5748	24.26	1032.7020	32.68	0.93
Z21	0.1335	0.71	7.0269	1.95	0.3818	1.82	2144.12	12.34	2114.8390	17.35	2084.8607	32.4	0.93
Z24	0.0701	1.61	1.4446	2.45	0.1495	1.85	931.2847	32.98	907.6365	14.71	897.9478	15.52	0.76
Z25	0.0742	0.89	1.6954	2.29	0.1658	2.12	1046.221	17.86	1006.8130	14.65	988.8027	19.4	0.92
Z26	0.0722	0.82	1.6791	1.69	0.1687	1.48	991.733	16.62	1000.6451	10.77	1004.7177	13.78	0.88
Z30	0.0706	0.98	1.5056	2.17	0.1547	1.94	945.2829	20.05	932.6642	13.27	927.3334	16.77	0.89
Z34	0.0658	1.18	1.1546	2.07	0.1272	1.7	801.4074	24.78	779.4286	11.26	771.7750	12.36	0.82
Z35	0.0928	2.40	2.4133	3.74	0.1886	2.87	1483.716	45.39	1246.5718	26.85	1113.8944	29.38	0.77

Table 9. LA-ICP-MS U-Pb results for zoned zircons from leucosomes in metapelite of the Yaoundé series.

Sample	Isotopic ratios						Apparent ages						rho
	$^{207}Pb/^{206}Pb$	%2σ	$^{207}Pb/^{205}U$	2σ	$^{206}Pb/^{208}U$	2σ	$^{207}Pb/^{206}Pb$	2σ	$^{207}Pb/^{205}U$	2σ	$^{206}Pb/^{208}U$	2σ	
Z3 core	0.0514	6.24	0.6940	4.02	0.0980	3.14	257.1465	137.4	535.1780	11.21	602.6236	18.4	0.78
Z3 rim	0.0647	1.21	0.9043	3.64	0.1014	3.43	764.6318	25.51	654.0077	17.54	622.4003	20.35	0.94
Z4 core	0.0752	0.82	1.7795	1.98	0.1716	1.8	1073.652	16.38	1037.9923	12.84	1021.1423	16.99	0.91
Z4 rim	0.0524	6.32	0.6650	3.93	0.0921	2.13	301.5535	138.1	517.6816	12.1	567.9469	11.94	0.54
Z7 core	0.0756	1.38	1.7610	3.94	0.1690	3.69	1083.34	27.6	1031.1986	25.52	1006.7896	34.42	0.94
Z7 rim	0.0620	1.27	0.8475	2.64	0.0991	2.32	674.7792	27.25	623.2645	12.32	609.1674	13.47	0.88
Z8 rim	0.0604	2.30	0.8478	3.17	0.1018	2.18	617.074	49.6	623.4189	14.75	625.1686	12.99	0.69
Z8 core	0.0763	2.64	1.4847	6.29	0.1410	5.71	1104.207	52.7	924.1597	38.14	850.5465	45.47	0.91
Z12 core	0.0701	1.56	1.3590	4.58	0.1405	4.31	932.3045	31.94	871.4548	26.82	847.7063	34.25	0.94
Z12 rim	0.0615	1.09	0.9102	2.43	0.1073	2.18	657.5111	23.39	657.1412	11.77	657.0335	13.59	0.89
Z20 core	0.0724	0.81	1.7784	2.95	0.1782	2.84	996.8004	16.37	1037.6119	19.16	1057.0889	27.64	0.96
Z20 rim	0.0603	1.26	0.7989	2.59	0.0961	2.26	614.6519	27.27	596.1838	11.69	591.3409	12.79	0.87
Z32 core	0.0671	4.16	1.0508	2.97	0.1136	2.71	839.9745	84.22	729.2884	8.31	693.7953	17.9	0.91
Z32 rim	0.0604	0.97	0.8606	1.76	0.1033	1.47	619.5192	20.92	630.4761	8.28	633.5354	8.885	0.84
Z36rim	0.0732	1.11	1.6318	2.12	0.1618	1.8	1018.486	22.52	982.5622	13.34	966.5619	16.18	0.85
Z36 core	0.0762	1.54	1.8670	2.6	0.1777	2.1	1100.841	30.76	1069.4846	17.21	1054.1738	20.41	0.81

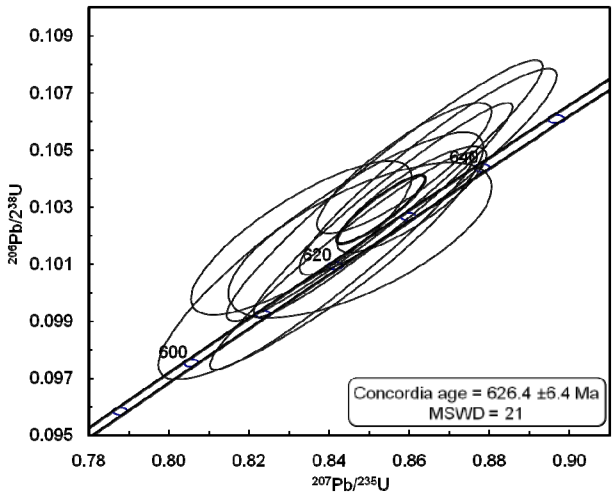

Figure 16. U-Pb Concordia diagram ages for zircons from leucosomes in metapelite of the Yaoundé series.

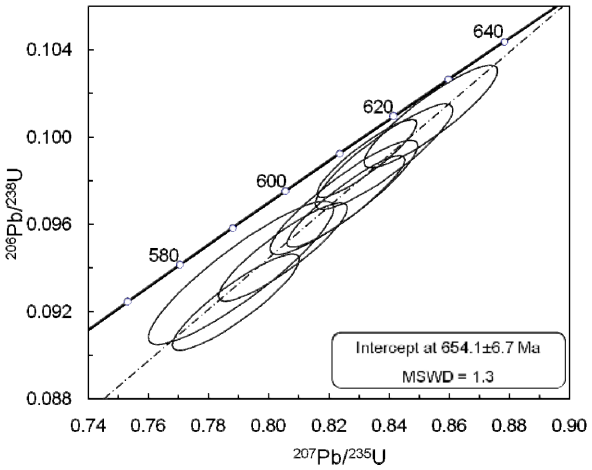

Figure 17. U-Pb Discordia diagram for zircons from leucosomes in metabasite of the Yaoundé series.

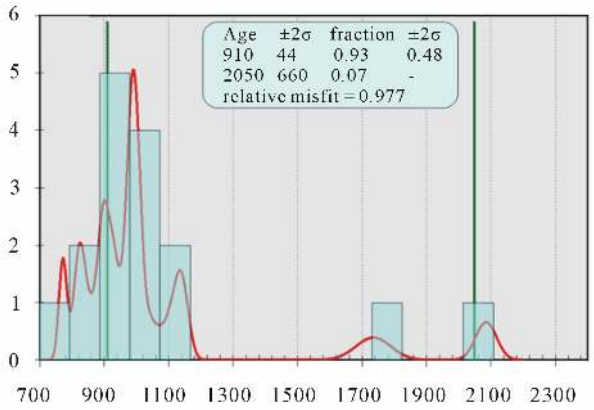

(a)

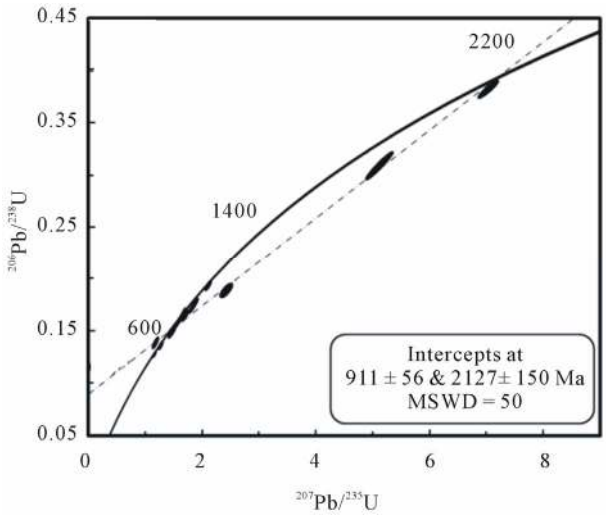

(b)

Figure 18. (a) Histogram of ages showing the different thermal event recorded by zoned zircons from leucosomes in metapelite of the Yaoundé series; (b) U-Pb Discordia diagram ages for these zircons.

from melting of metagreywacke. The difference between the two types of leucosomes could be linked to the difference in the composition of their source and the probable contamination during transportation of the melting material (displacement and injection of magmatic liquids). Thus the melting phenomenon observed in the Yaoundé series has not only affected the metapelitic rocks of this series but also the metagreywacke of the upper part of the crust as proposed in the other domains of the PANEFB. The proposed source for the leucosome of theYaoundé series is similar to that for the Akum-Bamenda leucogranites [4] and for the two-mica granitoids of Bafoussam area [21].

5.2. Comparison with the Granitoids of the PANEFB

The leucosomes of the Yaoundé series are silica-rich (71.91 - 74.41 wt% SiO_2; **Table 10**). The alkali concentration ($Na_2O + K_2O$ =3.53 - 9.11 wt%) and the variable K_2O/Na_2O ratios between 0.6 and 2 are characteristics of the high-K calc-alkaline to shoshonitic series (**Figure 21(a)**) as proposed for the granitoids of the central domain of the PANEFB [4,21-24,61-63]. The leucosomes of the Yaoundé series are peraluminous with the characteristics of S-type (*in situ* leucosomes) and I-type (injected leucosomes) granite. In the alumina index comparison diagram (**Figure 21(b)**), the *in situ* leucosomes show similar composition with Akum-Bamenda leucogranites [4] and two-mica granitoids of Bafoussam [21] whereas injected leucosomes are closer to the Banefo-Mvoutsaha granitoids [22] and to high-K calc-alkaline granitoids of Bapa-Batié [24]. These leucosomes can therefore be considered as peraluminous granite associated to the orogenic belt such as those described in [47-

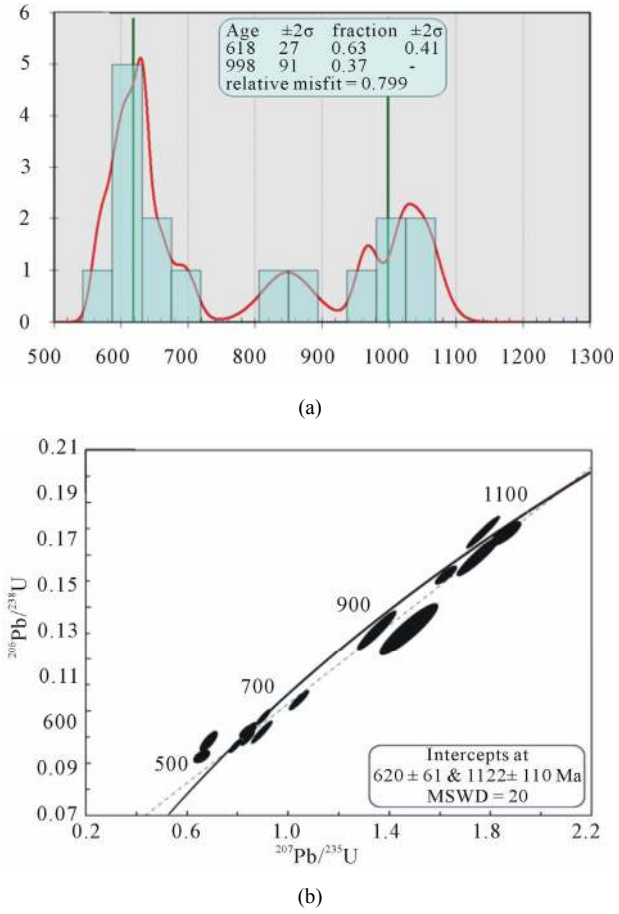

Figure 19. (a) Histogram showing the different thermal event recorded by no zoned from leucosomes in metapelite of the Yaoundé series; (b) U-Pb Discordia diagram ages for these zircons.

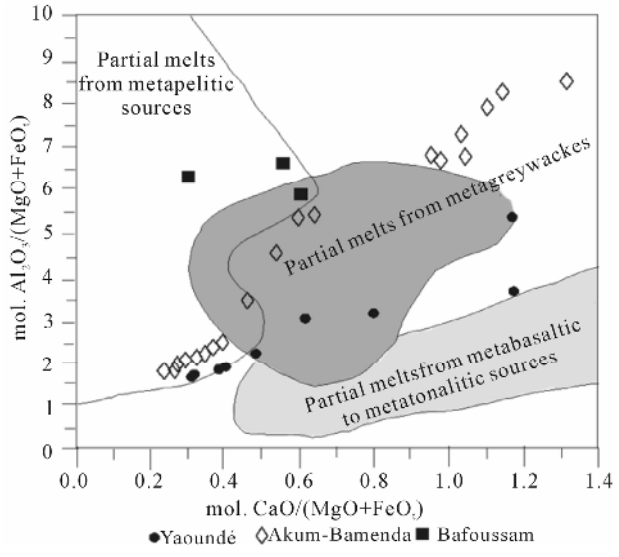

Figure 20. Molar CaO/(MgO + FeOt) vs Al_2O_3/(MgO + FeOt) diagram showing the same sources for Yaoundé leucosomes, Akum-Bamenda leucogranites and two-micas granitoids of Bafoussam.

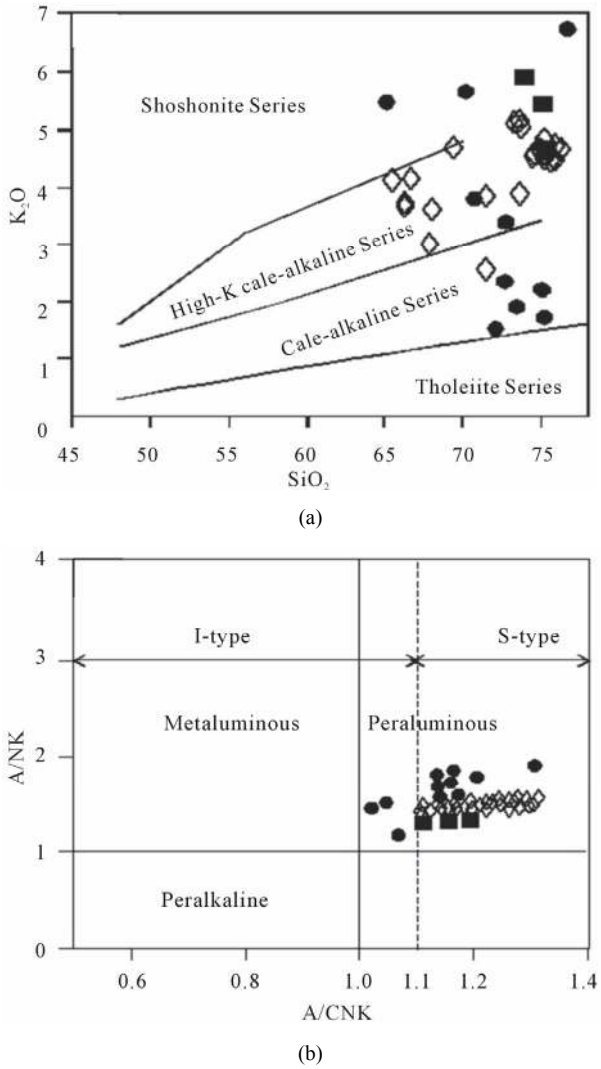

Figure 21. SiO_2 vs K_2O (a) and molar A/NK vs A/CNK (b) diagrams showing the same calc-alkaline, high-K to shoshonitic affinity, peraluminous character of the Yaoundé leucosomes, Akum-Bamenda leucogranites and two-micas granitoids of Bafoussam.

49].

The average Sr contents of Yaoundé leucosomes (218 ppm in *in situ* leucosomes, 410.63 ppm in injected leucosomes) are closer to those of Akum-Bamenda leucogranites (307.39 ppm, **Table 10**), high-K calc-alkaline granitoids of Bapa-Batié (111 - 609 ppm) and Tonga (281 - 780 ppm). The REE patterns of Yaoundé leucosomes and those of the granitoids of the central domain of the PANEFB are strongly parallel (**Figure 22**).These spectra show that the leucosomes of the Yaoundé series, as the other granitoids of the PANEFB, are strongly fractionated, with HREE depletion and LREE enrichment. However, the Yaoundé *in situ* leucosomes are more depleted in LREE and enriched in HREE than the Akum-Bamenda leucogranites and the two-mica granitoids of

Table 10. Compared average chemical analyses of the Yaoundé leucosomes, Akum-Bamenda leucogranite and two-micas granitoids of Bafoussam.

	Yaoundé leucosomes		PANEFB Leucogranites	
Rocks	***In situ***	**Injected**	**Akum-Bamenda Leucogranites***	**Two-mica ganitoids of Bafoussam****
SiO_2	74.41	71.96	71.17	73.10
Al_2O_3	12.29	15.59	15.81	14.47
Fe_2O_3	3.59	1.15	2.43	1.44
MnO	0.06	0.02	0.04	0.04
MgO	1.59	0.38	0.51	0.22
CaO	1.86	2.12	1.07	0.67
Na_2O	2.92	3.57	3.87	3.29
K_2O	1.69	3.99	4.21	5.09
TiO_2	0.53	0.27	0.29	0.17
P_2O_5	0.01	0.00	0.09	0.10
LOI	0.66	0.53	0.55	0.84
Rb	43.33	79.63	201.38	385.67
Sr	218.00	410.63	307.39	86.00
Zr	124.67	78.75	201.34	104.33
Nb	3.67	0.63	27.22	24.33
Y	20.83	12.50	48.41	13.33
La	16.36	24.60	29.99	44.87
Ce	33.18	48.37	60.79	77.60
Nd	15.46	22.51	24.44	30.22
Sm	3.67	4.52	4.34	5.51
Eu	1.61	1.86	1.12	0.48
Gd	3.28	3.46	4.02	3.72
Dy	2.95	1.80	2.68	2.36
Er	1.72	0.48	1.28	1.00
Yb	1.88	0.38	1.01	0.98
Lu	0.30	0.08	0.14	0.14
K/Rb	157.67	480.13	209.26	131.98
Rb/Sr	0.13	0.21	0.83	4.48
Ca/Sr	35.26	36.69	34.65	77.52
(Ce/Sm)N	2.14	3.19	3.31	3.32
(Gd/Yb)N	1.43	7.37	3.21	3.04
(Ce/Yb)N	4.74	36.42	15.43	20.20
Eu/Eu*	1.45	4.24	0.83	0.33

*Average of whole rock analyses of [4]; **Average of whole rock analyses of [21].

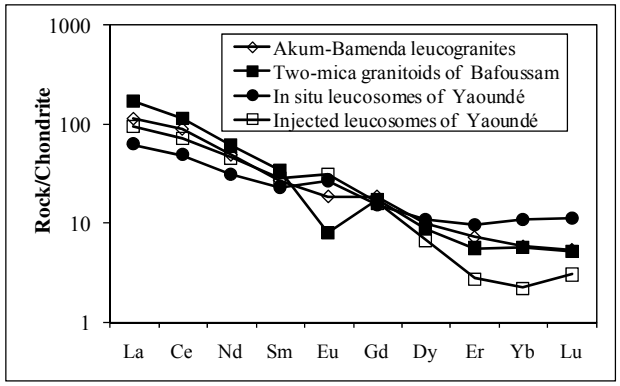

Figure 22. Chondrite-normalized REE comparison patterns for the Yaoundé leucosomes, Akum-Bamenda leucogranites and two-micas granitoids of Bafoussam.

Bafoussam. The REE patterns also show positive Eu anomalies for the Yaoundé leucosomes and negative to null Eu anomalies for the Akum-Bamenda leucogranites and the two-mica granitoids of Bafoussam. This contrasting Eu behaviour can be attributed to the difference in the geodynamic setting (tectono-metamorphic context in Yaoundé and tectono-magmatic context in the other domain of the PANEFB) of the emplacement of these granitoids.

5.3. Uniqueness of the Melting/Magmatism during the Pan-African Orogeny

The Palaeoproterozoic protolith (2127 Ma) of Yaoundé series underwent metamorphism between 1122 and 911 Ma. The Nd isotopic signature confirms the presence of late Paleoproterozoic to Archean relics in the central domain of the PANEFB [3,19,20,64-66]. In the SE of Tibati-Banyo shear zone, Pan-African granitoids derived from melting of a Paleoproterozoic crust with low participation of juvenile magma [3,18,62,66,67]. These observations confirm the initial existence of Paleoproterozoic formations in the three domains of the PANEFB in Cameroon.

The melting or the magmatism responsible for the leucosomes emplacement in the Yaoundé series occurred between 658 and 620 Ma. This magmatism is contemporaneous:

1) In the central domain, with the emplacement of two-mica granitoids of Bafoussam (564 - 558 Ma, EMP age; [21]), high-K calc-alkaline granitoids of Bapa-Batié (619 - 600 Ma, U-Pb age on zircon; [24]), and synkinematic granitoids of Tonga (618 Ma, U-Pb age on zircon; [19]);

2) In the northern domain, with the Pan-African (630 Ma, U-Pb age on zircon; [15]) calc-alkaline Syn-D_2 plutonism (diorite, granodiorite and tonalite);

3) In the eastern Cameroon, with the continental

magmatism responsible for the emplacement of Pan-African (614 ± 41 Ma) peraluminous granite and diorite, orthogneisses at 621 ± 13 Ma [25]. These orthogneisses are very abundant at the Cameroon-Central African Republic boundary.

For the above observations, the following interpretations could be made:

1) The high-K calc-alkaline to shoshonitic affinity of granitoids is observed in both central domain [4,19,21, 22,24,63], northern domain [15] and southern domain (as revealed by this work) of the PANEFB. With the ubiquity of the high-K calc-alkaline affinity in the PANEFB, we suggest that a former crust, widespread from the south to the north, was involved in the genesis of these rocks as outlined in [3,5,6];

2) The generalization of magmatism or melting in the whole PANEFB during the Pan-African orogeny between 592 and 658 Ma;

3) The existence of two sources (metapelite and metagreywacke sources) for the peraluminous granitoids of the PANEFB.

All these interpretations allow us to propose, in addition to metamorphism and tectonics, the existence of a unique magmatic event along the entire PANEFB in Cameroon.

6. Conclusions

The main conclusions obtained from this study are the following:

1) The Yaoundé series is composed of metasediment and metabasite which have been metamorphosed during Tonien-Stenien (911 - 1127 Ma) period.

2) These rocks have been affected by a melting responsible for the S-type and I-type peraluminous leucosomes emplacement. These leucosomes are calc-alkaline, high-K to shoshonitic affinity similar to the other granitoids of the PANEFB.

3) Geochemical data reveal that *in situ* leucosomes derived from the melting of the host metapelite whereas injected leucosomes derived from the melting of metagreywacke. These sources are similar to those of granitoids from central and northern domains of the PANEFB.

4) The melting responsible for the genesis of leucosomes in the Yaoundé series took place between 592 and 658 Ma as the magmatism responsible for the emplacement of granitoids in the other domains the PANEFB.

5) There is therefore uniqueness of melting and magmatism all over the PANEFB as the uniqueness observed in metamorphic and tectonic aspects.

7. Acknowledgements

The authors thank the Institute für Minerologie of University of Freiberg (Germany) and the Laboratory of Geochronology of the University of Brasilia (Brazil) for providing many facilities for EMP monazite dating and LA-ICP-MS U-Pb dating respectively. This is a contribution to IGCP project 616.

REFERENCES

[1] M. Pichavent, D. J. Kontak, L. Briqueu, J. V. Herrera and A. H. Clark, "The Miocene-Pliocene Macusani Volcanic, SE Peru. II. Geochemistry and Origin of a Peraluminous Magma," *Contribution to Mineralogy and Petrology*, Vol. 100, No. 3, 1988, pp. 325-338.

[2] M. Pichavent, D. J. Kontak, J. V. Herrera and A. H. Clark, "The Miocene-Pliocene Macusani Volcanic, SE Peru I. Mineralogy and Magmatic Evolution of a Two Mica Aluminosilicate Bearing Ignimbrite Suite," *Contribution to Mineralogy and Petrology*, Vol. 100, No. 3, 1988, pp. 300-324.

[3] J. P. Nzenti, E. L. T. Njiosseu and A. N. Nchare, "The Metamorphic Evolution of the Palaeoproterozoic High Grade Banyo Gneisses (Adamawa, Cameroon, Central Africa)," *Journal of the Cameroon Academy of Sciences*, Vol. 7, No. 2, 2007, pp. 95-109.

[4] J. P. Nzenti, B. Abaga, C. E. Suh and C. Nzolang, "Petrogenesis of Peraluminous Magmas from the Akum-Bamenda Massif, Pan-African Fold Belt, Cameroon," *International Geology Review*, Vol. 53, No. 10, 2011, pp. 1121-1149. doi:10.1080/00206810903442402

[5] D. T. Tchato, B. Schulz and J. P. Nzenti, "Electron Microprobe (EMP) Monazite Dating and P-T Data of the Neoproterozoic Metamorphic and Mylonitic Events in the Kekem Area, Cameroon North Equatorial Fold Belt," *Neues Jahbur of Paleontology*, Vol. 186, No. 1, 2009, pp. 95-109.

[6] J. P. Nzenti, P. Barbey, J. Macaudiere and D. Soba, "Origin and Evolution of the Late Precambrian High-Grade Yaoundé Gneisses (Cameroon)," *Precambrian Research*, Vol. 38, No. 2, 1988, pp. 91-109. doi:10.1016/0301-9268(88)90086-1

[7] T. Ngnotué, J. P. Nzenti, P. Barbey and F. M. Tchoua, "The Ntui-Betamba High Grade Gneisse: A Northward Extension of the Pan-African Yaoundé Gneisses in Cameroon," *Journal of African Earth Sciences*, Vol. 31, No. 2, 2000, pp. 369-381.

[8] J. P. Nzenti, P. Barbey, P. Jegouzo and C. Moreau, "Un Nouvel Exemple de Ceinture Granulitique dans une Chaîne Protérozoïque de Transition: Les Migmatites de Yaoundé au Cameroun," *Compte Rendu Académie des Sciences de Paris*, Vol. 299, No. 17, 1984, pp. 1197-1199.

[9] J. Penaye, S. F. Toteu, W. R. Van Schmus and J. P. Nzenti, "U-Pb and Sm-Nd Preliminary Geochronology Data on the Yaoundé Series, Cameroon: Re-Interpretation of the Granulitic Rocks as the Suture of Collision in the 'Centrafrican' Belt," *Comptes Rendus de l'Académie des Sciences de Paris*, Vol. 317, No. 2, 1993, pp. 789-794.

[10] S. F. Toteu, W. R. Van Schmus, J. Penaye and J. B. Nyobe, "U-Pb and Sm-Nd Evidence of Eburnian and Pan-African High Grade Metamorphism in Cratonic

Rocks of Southern Cameroon," *Precambrian Research*, Vol. 67, No. 3-4, 1994, pp. 321-347. doi:10.1016/0301-9268(94)90014-0

[11] S. Owona, B. Schulz, L. Ratschbacher, J. M. Ondoa, G. E. Ekodeck, F. M. Tchoua and P. Affaton, "Pan-African Metamorphic Evolution in the Southern Yaoundé Group (Oubanguide Complex, Cameroon) as Revealed by EMP Monazite Dating and Thermobarometry of Garnet Metapelites," *Journal of African Earth Sciences*, Vol. 59, No. 1, 2010, pp. 125-139. doi:10.1016/j.jafrearsci.2010.09.003

[12] J. P. Nzenti, "Pétrogenèse des Migmatites de Yaoundé (Cameroun): Eléments pour un Modèle Géodynamique de la Chaîne Panafricaine Nord-Equatoriale," These Doctorat, University of Nancy I, Nancy, 1987.

[13] P. Barbey, J. Macaudière and J. P. Nzenti, "High-Pressure Dehydration Melting of Metapelites: Evidence from Migmatites of Yaoundé (Cameroon)," *Journal of Petrology*, Vol. 31, No. 2, 1990, pp. 401-428.

[14] V. Ngako, "Evolution Métamorphique et Structurale de la Bordure Sud-Ouest de la 'Série de Poli', Segment Camerounais de la Chaîne Panafricaine," *Mémoire et documents du C.A.E.S.S.*, Vol. 5, 1986, 185 p.

[15] S. F. Toteu, A. Michard, J. M. Bertrand and G. Rocci "U/Pb of Precambrian Rocks from Northern Cameroon, Orogenic Evolution and Chronology of the Pan-African Belt of Central Africa," *Precambrian Research*, Vol. 37, No. 1, 1987, pp. 71-87. doi:10.1016/0301-9268(87)90040-4

[16] J. Penaye, S. F. Toteu, A. Michard, J. M. Bertrand and D. Dautel, "Reliques Granulitiques d'Age Protérozoïque Inférieur dans la Zone Mobile Panafricaine d'Afrique Centrale au Cameroun: Géochronologie U-Pb sur Zircons," *Comptes Rendus de l'Académie des Sciences de Paris*, Vol. 309, No. 2A, 1989, pp. 315-318.

[17] J. P. Nzenti, "Prograde and Retrograde Garnet Zoning at High Pressure and Temperature in Metapelitic and Grenatite Rocks from Yaoundé," *Journal of African Earth Sciences*, Vol. 15, No. 1, 1992, pp. 73-79. doi:10.1016/0899-5362(92)90008-Z

[18] J. P. Nzenti, P. Barbey and F. M. Tchoua, "Evolution Crustale au Cameroun: Eléments pour un Modèle Géodynamique de l'Orogenèse Néoprotérozoïque," In: J.-P. Vicat and P. Bilong, Eds., *Géologie et Environments au Cameroun*, *GEOCAM*, Vol. 2, 1999, pp. 397-407.

[19] E. L. T. Njiosseu, J. P. Nzenti, T. Njanko, B. Kapajika and A. Nédelec, "New U-Pb Zircon Ages from Tonga (Cameroon): Coexisting Eburnean-Transamazonian (2.1 Ga) and Pan-African (0.6 Ga) Imprints,"*Comptes Rendus Géosciences*, Vol. 337, No. 16, 2005, pp. 551-562. doi:10.1016/j.crte.2005.02.005

[20] A. A. Ganwa, W. Frisch, W. Siebel, G. E. Ekodeck, C. K. Shang and V. Ngako, "Archean Inheritances in the Pyroxene-Amphibole-Bearing Gneiss of the Méiganga Area (Central North Cameroon): Geochemical and Pb/Pb Age Imprints," *Comptes Rendus Geosciences*, Vol. 340, No. 4, 2008, pp. 211-222. doi:10.1016/j.crte.2007.12.009

[21] M. L. Djouka-Fonkwe, B. Schulz, J. P. Tchouankoué and C. Nzolang, "Geochemistry of the Bafoussam Pan-African I- and S-type Granitoids in Western Cameroon," *Journal of African Earth Sciences*, Vol. 50, No. 2-3, 2008, pp. 148-167. doi:10.1016/j.jafrearsci.2007.09.015

[22] G. D. K. Nono, J. P. Nzenti, C. E. Suh and S. Ganno, "Geochemistry of Ferriferous, High-K Calc-Alkaline Granitoids from Banefo-Mvoutsaha Massif (NE Bafoussam), Central Domain of the Pan-African Fold Belt, Cameroon," *The Open Geology Journal*, Vol. 4, No. 1, 2010, pp. 21-34.

[23] A. N. Nchare, J. P. Nzenti, E. L. T. Njiosseu, S. Ganno and T. Ngnotué, "Synkinematic Ferro-Potassic Magmatism from the Mekwene-Njimafofire Foumban Massif, along the Foumban-Banyo Shear Zone in Central Domain of Cameroon Pan-African Fold Belt," *Journal of Geology and Mining Research*, Vol. 2, No. 6, 2010, pp. 142-158.

[24] C. Chebeu, C. D. N. Nlend, J. P. Nzenti and S. Ganno, "Neoproterozoic High-K Calc-Alkaline Granitoids from Bapa-Batié, North Equatorial Fold Belt, Central Cameroon: Petrogenesis and Geodynamic Significance," *The Open Geology Journal*, Vol. 5, 2011, pp. 1-20. doi:10.2174/1874262901105010001

[25] D. Soba, A. Michard, S. F. Toteu, D. I. Norman, J. Penaye, V. Ngako, J. P. Nzenti and D. Dautel, "Données Géochronologiques Nouvelles (Rb-Sr, U-Pb et Sm-Nd) sur la Zone Mobile Panafricaine de l'Est-Cameroun: Age Protérozoique Supérieur de la Série de Lom," *Comptes Rendus de l'Académie des Sciences de Paris*, Vol. 312, No. 2, 1991, pp. 1453-1458.

[26] G. Njiekak, W. Dörr, J. P. Tchouankoue and G. Zulauf, "U-Pb Zircon and Microfabric Data of (Meta) Granitoids of Western Cameroon: Constraints on the Timing of Pluton Emplacement and Deformation in the Pan-African Belt of Central Africa," *Lithos*, Vol. 102, No. 3-4, 2008, pp. 460-477. doi:10.1016/j.lithos.2007.07.020

[27] K. Govindaraju and R. Montanary, "Routine Performance of a Matrix-Correction Free X-Ray Flurorescence Spectrometric Method for Rock Analysis," *X-ray Spectrometry*, Vol. 7, No. 3, 1978, pp. 148-151. doi:10.1002/xrs.1300070307

[28] K. Govindaraju, "Report (1980) on Three GIT-IWG Rock Reference Samples: Anorthosite from Greenland, AN-G; Basalte d'Essey-la-Cote, BE-N; Granite de Beauvoir, MA-N," *Geostandards Newsletters*, Vol. 4, No. 1, 1980, pp. 49-138. doi:10.1111/j.1751-908X.1980.tb00274.x

[29] B. M. Jahn, P. Vidal and G. R. Tilton, "Archean Mantle Heterogeneity: Evidence from Chemical and Isotopic Abundances in Archean Igneous Rocks," *Philosophical Transactions of the Royal Society*, Vol. 297, 1980, pp. 353-364. doi:10.1098/rsta.1980.0221

[30] B. Schulz, H. Brätz, K. Bombach and E. Krenn, "*In situ* Th-Pb Dating of Monazite by 266 nm Laser Ablation and ICP-MS with a Single Collector, and Its Control by EMP Analysis-Z. Angew," *Geology*, Vol. 35, No. 4, 2007, pp. 377-392.

[31] E. Jarosewich and L. A. Boatner, "Rare-Earth Element Reference Samples for Electron Microprobe Analysis," *Geostandards Newsletter*, Vol. 15, No. 2, 1991, pp. 397-399. doi:10.1111/j.1751-908X.1991.tb00115.x

[32] J. J. Donovan, J. M. Hanchar, P. M. Picolli, M. D. Schrier,

L. A. Boatner and E. Jarosewich, "A Re-Examination of the Rare-Earth-Element Orthophosphate Standards in Use for Electron-Microprobe Analysis," *Canadian Mineralogist*, Vol. 41, No. 1, 2003, pp. 221-232. doi:10.2113/gscanmin.41.1.221

[33] F. Finger and H. M. Helmy, "Composition and Total-Pb Model Ages of Monazite High Grade Paragneisses in the Abu Swayel Area, Southern Eastern Desert, Egypt," *Mineralogy and Petrology*, Vol. 62, No. 3-4, 1998, pp. 269-289. doi:10.1007/BF01178032

[34] J. M. Montel, S. Foret, M. Veschambre, C. Nicollet and A. Provost, "A Fast, Reliable, Inexpensive *in-Situ* Dating Technique: Electron Microprobe Ages of Monazite," *Chemical Geology*, Vol. 131, No. 1, 1996, pp. 37-53. doi:10.1016/0009-2541(96)00024-1

[35] M. J. Jercinovic and M. L. Williams, "Analytical Perils (and Progress) in Electron Microprobe Trace Element Analysis Applied to Geochronology: Background Acquisition, Interferences, and Beam Irradiation Effects," *American Mineralogist*, Vol. 90, No. 5, 2005, pp. 526-546. doi:10.2138/am.2005.1422

[36] B. Buhn, M. M. Pimentel, M. Matteini and E. L. Dantas, "High Spatial Resolution Analysis of Pb and U Isotopes for Geochronology by Laser Ablation Multi-Collector Inductively Coupled Plasma Mass Spectrometry (LA-MC-ICP-MS)," *Anais da Academia Brasiliera de Ciências*, Vol. 81, No. 1, 2009, pp. 1-16. doi:10.1590/S0001-37652009000100011

[37] S. E. Jackson, N. J. Pearson and W. L. Griffin, "The Application of Laser Ablation-Inductively Coupled Plasma-Mass Spectrometry to *in Situ* U-Pb Zircon Geochronology," *Chemical Geology*, Vol. 211, No. 1-2, 2004, pp. 47-69. doi:10.1016/j.chemgeo.2004.06.017

[38] F. Albarède, P. Telouk, J. Blichert-Toft, M. Boyet, A. Agranier and B. Nelson, "Precise and Accurate Isotopic Measurements Using Multiple Collector ICPMS," *Geochimical and Cosmochimical Acta*, Vol. 68, No. 12, 2004, pp. 2725-2744. doi:10.1016/j.gca.2003.11.024

[39] L. P. Black, S. L. Kamo, C. M. Allen, D. W. Davis, J. N. Aleinikoff, J. W. Valley, R. Mundil, I. H. Campbell, R. J. Korsch, I. S. William and C. Foudoulis, "Improved $^{206}Pb/^{238}U$ Microprobe Geochronology by the Monitoring of a Trace-Element-Related Matrix Effect: SHRIMP, ID-TIMS, LA-ICP-MS and Oxygen Isotope Documentation for a Series of Zircon Standards," *Chemical Geology*, Vol. 205, No. 1-2, 2004, pp. 115-140. doi:10.1016/j.chemgeo.2004.01.003

[40] J. S. Stacey and J. D. Kramers, "Approximation of Terrestrial Lead Isotope Evolution by a Two-Stage Mode," *Earth Planetary Science Letters*, Vol. 26, No. 2, 1975, pp. 207-221. doi:10.1016/0012-821X(75)90088-6

[41] K. R. Ludwig, "Users Manual for Isoplot/Ex rev. 2.49. A Geochronological Toolkit for Microsoft Excel," *Berkeley Geochronology Center Special Publication*, Vol. 1a, 2001, pp. 1-55.

[42] K. R. Ludwig, "User's Manual for Isoplot/Ex v. 3.00. A Geochronological Toolkit for Microsoft Excel," *BGC Special Publication*, Vol. 4, No. 1, 2003, pp. 1-71.

[43] E. A. K. Middlemost, "Magmas and Magmatic Rocks," Longman, London, 1985.

[44] J. M. Bertrand, C. Dupuy, J. Dostal and I. Davidson, "Geochemistry and Geotectonic Interpretation of Granitoids from Central Iforas (Mali, West Africa)," *Precambrian Research*, Vol. 26, No. 3-4, 1984, pp. 265-283. doi:10.1016/0301-9268(84)90004-4

[45] R. Ayuso and J. G. Arth, "The Northeast Kingdom Batholiths, Vermon: Magmatic evolution and Geochemical Constraints on the Origin of Acadian Granitics Rocks," *Contribution to Mineralogy and Petrology*, Vol. 111, No. 1, 1992, pp. 1-23. doi:10.1007/BF00296574

[46] K. Suzuki, M. Adachi and I. Kajisuka, "Electron Microprobe Observations of Pb Diffusion in Metamorphosed Detrital Monazites," *Earth and Planetary Sciences Letters*, Vol. 128, No. 3-4, 1994, pp. 391-405. doi:10.1016/0012-821X(94)90158-9

[47] M. P. Searle, R. R. Parrish, K. V. Hodges, A. Hurford, M. W. Ayres and M. J. Whitehouse, "Shisha Pangma Leucogranite, South Tibetan Himalayan: Field Relations, Geochemistry, Age, Origin and Emplacement," *Journal of Geology*, Vol. 105, No. 3, 1997, pp. 295-317. doi:10.1086/515924

[48] B. Barbarin, "A Review of the Relationships between Granitoids Types, Their Origin and Their Geodynamics Environments," *Lithos*, Vol. 46, No. 4, 1999, pp. 605-626. doi:10.1016/S0024-4937(98)00085-1

[49] P. I. Nabalek and M. Liu, "Petrology and Thermal Constraints on the Origin of Leucogranites in Collisional Orogens," *Transactions of the Royal Society of Edinburgh, Earth Sciences*, Vol. 95, No. 1, 2004, pp. 73-85. doi:10.1017/S0263593304000094

[50] C. F. Miller, "Are Strongly Peraluminous Magmas Derived from Pelitic Sedimentary Sources?" *Journal of Geology*, Vol. 93, No. 6, 1985, pp. 673-689. doi:10.1086/628995

[51] A. E. P. Douce, "Experimental Generation of Hybrid Silicic Melts by Reaction of High Al Basalt with Metamorphic Rocks," *Journal of Geophysical Research*, Vol. 100, No. B8, 1995, pp. 623-639.

[52] P. Le Fort, M. Cuney, C. Deniel, C. France-Lanord, S. M. F. Sheppard, B. N. Upreti and P. Vidal, "Crustal Generation of the Himalayan Leucogranites," *Tectonophysics*, Vol. 134, No. 1, 1987, pp. 39-57. doi:10.1016/0040-1951(87)90248-4

[53] A. J. R. White and B. W. Chappell, "A-Type Granites: Geochemical Characteristics, Discrimination and Petrogenesis," *Contribution to Mineralogy and Petrology*, Vol. 95, No. 4, 1987, pp. 407-419. doi:10.1007/BF00402202

[54] N. B. W. Harris and S. Inger, "Trace Element Modelling of Pelitte-Derived Granites," *Contributions to Mineralogy and Petrology*, Vol. 110, No. 1, 1992, pp. 46-56. doi:10.1007/BF00310881

[55] B. J. Williamson, H. Downes, M. F. Thirlwall and A. Beard, "Geochemical Constraints on Restite Composition and Unmixing in the Velay Anatectic Granite, French Massif Central," *Lithos*, Vol. 40, No. 2-4, 1997, pp. 295-319. doi:10.1016/S0024-4937(97)00033-9

[56] M. Cuney, P. Sabaté, P. Vidal, M. Marinho and H. Com-

ceiçao, "The 2 Ga Peraluminous Magmatism of Jacobina-Contendas Mirante Belt (Bahia-Brasil): Major- and Trace-Element Geochemistry and Metallogenic Potential," *Journal of Volcanology and Geothermal Research*, Vol. 44, No. 1-2, 1990, pp. 123-141. doi:10.1016/0377-0273(90)90015-8

[57] D. Vielzeuf and J. Hollaway, "Experimental Determination of the Fluid-Absent Melting Relations in the Pelitic System," *Contribution to Mineralogy and Petrology*, Vol. 98, No. 3, 1988, pp. 257-276. doi:10.1007/BF00375178

[58] A. E. P. Douce and A. D. Johnston, "Phase Equilibria and Melt Productivity in the Politic System: Implications for the Origin of Peraluminous Granitoids and Aluminous Granulites," *Contribution to Mineralogy and Petrology*, Vol. 107, No. 2, 1991, pp. 202-218. doi:10.1007/BF00310707

[59] B. R. Frost, C. G. Barnes, W. J. Collins, R. J. Arculus, D. J. Ellis and C. D. Frost, "A Geochemical Classification for Granitic Rocks," *Journal of Petrology*, Vol. 42, No. 11, 2001, pp. 2033-2048. doi:10.1093/petrology/42.11.2033

[60] F. F. Altherr, A. Holl, E. Hegner, C. Langer and H. Kreuser, "High-Potassium, Calc-Alcaline I-Type Plutonism in the European Variscides: Nothern Vosges (France) and Northern Schwarzwald (Germany)," *Lithos*, Vol. 50, No. 1-3, 2000, pp. 51-73. doi:10.1016/S0024-4937(99)00052-3

[61] C. Nzolang, H. Kagami, J. P. Nzenti and F. Holz, "Geochemistry and Preliminary Sr-Nd Isotopic Data on the Neoproterozoic Granitoids from the Bantoum Area, West Cameroon: Evidence for a Derivation from a Paleoproterozoic to Archean Crust," *Polar Geoscience*, Vol. 16, 2003, pp. 196-226.

[62] T. Njanko, A. Nedélec and P. Affaton, "Synkinematic High-K Calc-Alkaline Plutons Associated to the Pan-African Central Cameroon Shear Zone (West-Tibati area): Petrology and Geodynamic Significance," *Journal of African Earth Sciences*, Vol. 44, No. 4-5, 2006, pp. 494-510. doi:10.1016/j.jafrearsci.2005.11.016

[63] J. P. Nzenti, B. Kapajika, G. Wörner and R. T. Lubala, "Synkinematic Emplacement of Granitoids in a Pan-African Shear Zone in Central Cameroon," *Journal of African Earth Sciences*, Vol. 45, No. 1, 2006, pp. 74-86. doi:10.1016/j.jafrearsci.2006.01.005

[64] J. P. Nzenti, P. Barbey, J. M. Bertrand and J. Macaudière, "La Chaîne Panafricaine au Cameroun: Cherchons Suture et Modèle!" 15*th Réunion des Sciences de la Terre*, Nancy, 26-28 April 1994.

[65] A. A. Ganwa, W. Frisch, W. Siebel, G. E. Ekodeck, C. K. Shang, J. M. Ondoa, M. Satir and J. T. Numbem, "Zircon Pb/Pb Evaporation Ages of Panafrican Metasedimentary Rocks in the Kombé-II Area (Bafia Group, Cameroon): Constraints on Protolith Age and Provenance," *Journal of African Earth Sciences*, Vol. 51, No. 2, 2008, pp. 77-88. doi:10.1016/j.jafrearsci.2007.12.003

[66] A. A. Ganwa, W. Siebel, C. K. Shang, N. Seguem and G. E. Ekodeck, "New Constraints from Pb-Evaporation Zircon Ages of the Méiganga Amphibole-Biotite Gneiss, Central Cameroon, on Proterozoic Crustal Evolution," *International Journal of Geosciences*, Vol. 2, No. 2, 2011, pp. 138-147.

[67] J. P. Nzenti, "Neoproterozoic Alkaline Meta-Ignous Rocks from the Pan-African North Equatorial Fold Belt (Yaoundé, Cameroon): Biotitites and Magnetite Rich Pyroxenites," *Journal of African Earth Sciences*, Vol. 26, No. 1, 1998, pp. 37-47. doi:10.1016/S0899-5362(97)00135-8

